

Dark Matter Candidates of a Very Low Mass

Kathryn M. Zurek

We review dark matter (DM) candidates of a very low mass appearing in the window below the traditional weakly interacting massive particle ($m_\chi \lesssim 10$ GeV) and extending down to $m_\chi \gtrsim 1$ meV, somewhat below the mass limit at which DM becomes wavelike. Such candidates are motivated by hidden sectors such as hidden valleys, which feature hidden forces and rich dynamics, but have evaded traditional accelerator searches for New Physics because of their relatively weak coupling to the Standard Model (SM). Such sectors can still be detected through dedicated low-energy colliders, which, through their intense beams, can have sensitivity to smaller couplings, or through astrophysical observations of the evolution of DM halos and stellar structures which, through the Universe's epochs, can be sensitive to small DM interactions. We also consider mechanisms whereby the DM abundance is fixed through the interaction with the SM, which directly motivates the search for light DM in terrestrial experiments. The bulk of this review is dedicated to the new ideas that have been proposed for direct detection of such DM candidates of a low mass through nuclear recoils, electronic excitations, or collective modes such as phonons and magnons. The rich tapestry of materials and modes in the condensed matter landscape is reviewed along with specific prospects for detection.

CONTENTS

I. Hidden Sector Dark Matter: An Introduction	3
II. Models of Light Dark Matter: a Brief Overview	7
III. Mechanisms for Light Dark Matter Relic Abundance	9
A. Simplified Models in Direct Detection	9
B. Thermal Freeze-Out of Symmetric Dark Matter	11
C. Thermal Freeze-Out of Asymmetric Dark Matter	14
D. Freeze-In	16
E. Strongly Interacting Massive Particles and Elastically Decoupling Relics	17
IV. Astrophysical, Cosmological, and Accelerator Probes	18
A. Big Bang Nucleosynthesis	18
B. Cosmic Microwave Background	19
C. Large-Scale Structure	20
D. Stellar Evolution and Cooling	21
E. Accelerator Probes of Light Hidden Sectors	22
V. Direct detection of light-particle dark matter	23
A. Targets and Excitations for Dark Matter Interactions	25
B. Quantum Mechanics of Dark Matter Scattering	27
1. Nuclear recoils	29
2. Electronic excitations	29
3. Single Phonon excitations	32
C. In-Medium Effects	36
VI. Generalized Dark Matter Interactions	36
A. Effective Field Theory of Dark Matter Scattering with Collective Excitations	36
B. Target Response to Dark Matter Absorption	39
VII. Conclusion	41

Disclosure Statement	43
Acknowledgments	43
References	43

I. HIDDEN SECTOR DARK MATTER: AN INTRODUCTION

In the search for DM candidates, a few considerations enter—most notably that any DM candidate must satisfy observational evidence. This begins with the observed DM density, which is fixed most precisely at the epoch of the cosmic microwave background (CMB, when the Universe was approximately 380,000 years old, at a redshift of $z \sim 10^3 - 10^4$). From that epoch until today, it is known—on the largest scales of the Universe, from the formation of galaxies and clusters of galaxies as well as galactic rotation curves—that DM density (ρ) must dilute with the expanding volume of the Universe, $\rho = \rho^0(1+z)^3$ (with ρ^0 the density today), and must have very weak interactions with the baryons (so as not to disturb CMB baryon acoustic oscillations) and also with itself so that the structure of galaxies remains approximately oblate (neither a perfect sphere nor a disk). That is, *on average*, the DM must have a cold equation of state ($w = 0$) at least since the time the Universe was approximately 380,000 years old and must have weak enough interactions with itself and with ordinary matter that the gravitational force dominates the formation of bound structures, and not other forces like baryonic pressure. Beyond this broad set of facts, little is known about the DM. For a classic review of the evidence for DM, we refer the reader to, for example, Reference [1].

Around the time that these facts about the Universe were becoming broadly accepted (in the 1980s), particle physics was itself struggling with some puzzles that mostly concerned questions of naturalness. It turned out that solving these problems of naturalness in the Standard Model (SM) of particle physics naturally produced two DM candidates. The first of these candidates is the weakly interacting massive particle (WIMP), which appears as part of the solution to the question of why the Higgs boson mass (and hence weak forces) is so light; by extension, the WIMP mass is typically at the weak scale, and WIMPs have weak interactions, making them very susceptible to detection with the barrage of experiments that

probe the weak scale. The second of these candidates is the axion, a possible solution to the question of why there is so little CP violation in the strong interactions. The axion has interactions that are much weaker than weak (corresponding to a mass scale of 10^9 GeV up to the Planck scale), but its much lower mass, and hence much higher number density, gives a boost to the detection probability, typically in electromagnetic cavities that exploit the coherent enhancement of a wavelike state such as axion DM. Both WIMPs and axions could be produced in the early Universe (thermally and non-thermally, respectively) in an abundance consistent with observations. Multiple experimental efforts are underway to search for these DM candidates. Because they are part of the solution to the SM's problems, they have interactions with the SM that allow one to predict detection in a sufficiently sensitive device with ordinary particles. Well-defined predictions are appealing to the intrepid DM hunter. We refer the reader to recent reviews ([2, 3]) that describe these ongoing efforts.

However, the narrow focus on these two candidates sidesteps the fact that, from an observational point of view, a huge mass range of DM particles and almost as large a range of interactions are observationally possible. On the low mass end, DM can be as light as is consistent with the formation of structure on dwarf-galaxy scales, which implies that the de Broglie wavelength of the DM must be shorter than a typical dwarf galaxy size, implying $m_\chi \gtrsim 10^{-22}$ eV. On the upper mass end, DM is not observed to be clumpy (or grainy) in measurements of the Lyman- α forest; this implies that DM should have a mass $m_\chi \lesssim 10^3 M_\odot$ (for reference, $1 M_\odot \sim 10^{57}$ GeV) to be sufficiently smooth (see Reference [4], in which shot noise fluctuations from primordial black hole DM were considered). Any mass in-between is consistent with observations.

Once one releases the requirement that the DM solve one of the SM's problems, a hidden world of possibilities opens, subject only to the requirement that the DM

- have the observed abundance,
- dilute as a cold non-relativistic state after the CMB epoch,
- have its interactions on large scales be dominated by gravity, and
- satisfy the requirement that DM-baryon interactions not damp baryons after the CMB epoch and not affect the formation of nuclei in the early Universe.

In fact, there is not even a requirement that the hidden world have only one dark state, that it have self-interactions much weaker than baryonic, or that *all* of the dark sector be nonrelativistic.

The structure of a hidden sector (also known as a hidden valley or dark sector) is shown schematically in Figure 1. The barrier between the SM and the hidden sector represents the interaction between the two sectors; a higher barrier represents a weaker interaction. The highest barrier is the weakest force of all, gravity. To detect DM through individual particle interactions with the SM, there must be other, much lower barriers; these are represented as lower peaks. The mass scale of the hidden sector, represented by the height of the “floor,” is unknown.

One is tempted to become overwhelmed by such a huge mass range of DM, the types of dark sectors, and their interactions. Thus, it helps to break things down according to the physics governing the DM masses and interactions. In this article, we focus on a mass range of particle DM that is motivated, by its relic abundance, to have large enough interactions with the SM to be detectable through particle interactions. When the DM is heavier than approximately 10 TeV, setting its relic abundance through interactions with the SM is challenging (due to constraints from perturbative unitarity, as explicitly shown below). For heavier-mass DM, one can use gravitational means (*e.g.* pulsar timing [5] or the unique motions of stars [6]) or an additional DM-SM fifth force to search for such candidates [7], often through astrophysical means. On the other end of the mass scale, when the DM is lighter than ~ 1 eV, it behaves more like a wave than an individual particle. Detection techniques in this ultralight mass regime focus on using coherence, often in electromagnetic cavities or with other AMO techniques [8]. While this is a vibrant area of research, it is not the focus of this article.

We focus on hidden-sector DM candidates in the low mass range, whose relic abundance is still naturally set by its interactions with the SM, where there is motivation to search for such a state through detection of individual particles in terrestrial experiments. This implies a DM mass range between approximately a few keV (below which DM that is produced by its particle interactions with the SM will be too warm to cluster appropriately; see *e.g.* Reference [9]) and approximately 10 GeV, just below the weak scale. Because these hidden-sector states have masses below the weak-scale interactions, making for a low mass floor in

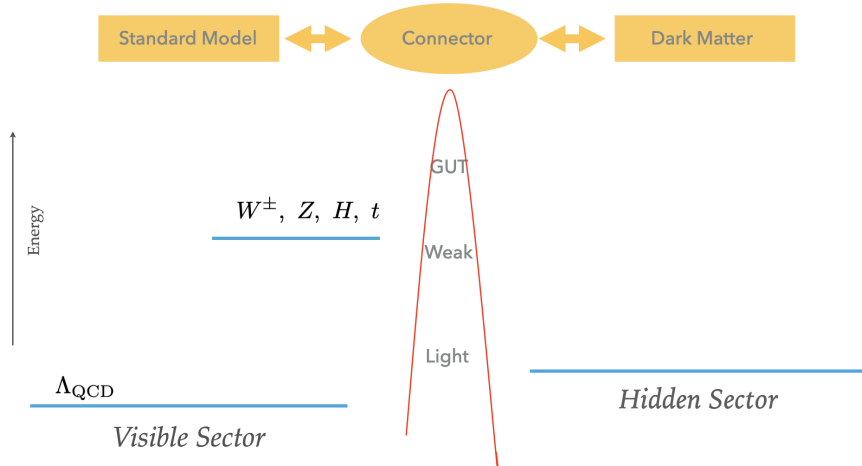


Figure 1. Schematic of hidden-sector dark matter. The barrier in the center of the figure represents the interaction (from a GUT, weak scale, or light mediators) between the two sectors; a higher barrier represents a weaker interaction. The mediator connects the visible and hidden sectors, and the different heights of the floors in the two sectors reflect the mass gap. In the visible sector we have the Standard Model, with a mass gap for the baryons of around a GeV, while in the dark matter sector, the scale of the mass gap and the structure of the states there are unknown. Abbreviation: GUT, grand unified theory.

the schematic of Figure 1, we refer to these DM models as hidden-valley DM (HVDM) or hidden-sector DM (HSDM).

The outline of the rest of this review is as follows. In the next section, we review how DM candidates of a very low mass can naturally have their relic abundance set through interactions with the SM. We characterize the various kinds of mechanisms that are often used in the literature to set the relic abundance. We then turn to examining astrophysical and cosmological probes for HVDM, a discussion that by itself sheds a light on where DM might be detected in terrestrial experiments. Then we turn to the main subject of the article, terrestrial probes for HVDM, and focus mostly on direct detection experiments. Novel probes must be invented to search for HVDM because the traditional nuclear recoil probes of WIMP DM are ineffective. More specifically, this implies using the wealth of collective modes (such as phonons and magnons) that are available in condensed matter systems. We also briefly review other kinds of terrestrial probes for HVDM, such as accelerator-based experiments.

II. MODELS OF LIGHT DARK MATTER: A BRIEF OVERVIEW

The broad range of hidden-sector models necessitates a tight selection of theory for this review. We focus here on direct detection prospects in terrestrial experiments and, therefore, on interactions with the SM that could be detected. These interactions are the most motivated when they also set the relic abundance, as discussed in the next section. In the dark sector itself, the structure is relatively unconstrained, especially if the mass gap in the hidden sector is $\gtrsim 10$ MeV, where constraints from big bang nucleosynthesis (BBN) from a thermalized hidden sector can be most easily satisfied. For example, the hidden sector could be [10, 11]

- a QCD-like theory with F -flavors and N -colors, with only light or heavy quarks, or adjoint quarks;
- a QED-like theory with only massive force mediators;
- a pure-gluon theory;
- a remnant from supersymmetry breaking;
- a partially Higgsed $SU(N)$ theory;
- a Seiberg duality cascade;
- unparticles; or
- a sector arising from a Randall–Sundrum or Klebanov-Strassler throat in extra dimensions.

Hidden sectors with such structures will naturally give rise to DM self-interactions. Strongly coupled hidden sectors have weakly coupled duals, so it is also possible to write effective Lagrangians in terms of weakly coupled scalars, fermions, and vector mediators [12]. To take a particularly simple example, the dark sector could be a QCD-like theory with two colors, two light flavors, and no heavy flavors [10]. Such a hidden sector has gapped degrees of freedom and the hidden pions π_v^\pm and π_v^0 . Note that the plus-minus symbol here does not denote electric charge but rather charge under a new global symmetry in the hidden sector

that stabilizes the pions carrying the global symmetry π_v^\pm . The relic abundance is fixed by the rate of the annihilation process

$$\pi_v^+ \pi_v^- \rightarrow \pi_v^0 \pi_v^0, \quad (1)$$

with $\pi_v^0 \rightarrow f\bar{f}$ decaying, for example, to SM fermions to which the dark-sector states couple via the connector state. This structure also appears in secluded DM models [13, 14].

Note that it is quite natural in such theories for the DM to have an asymmetric relic abundance, as proposed in Reference [15]. For example, a large enough asymmetry (or chemical potential) between π_v^+ and its anti-particle in the example above changes the cosmology and the computation of the relic abundance, as discussed in more detail below. The reader also may consult Reference [16] for a discussion of HVDM/HSDM in the context of asymmetric DM. This general framework of asymmetric DM triggered a slew of model building, from atomic [17], quirky [18] and glueball [19] DM to the WIMPless [20] and strongly interacting massive particle (SIMP) [21] “miracles”.

Hidden sectors also naturally allow for “portals” between the two sectors, through which the DM interacts with the SM, giving rise to signatures in terrestrial experiments. Since the DM is electrically neutral, there are two natural portals involving dimension-4 operators:

- A vector portal that includes a dark photon A'_μ kinetically mixed with the photon [22] (see Reference [23] for an application to DM):

$$\mathcal{L}_{A'} \supset -\frac{1}{2}m_{A'}^2 - \frac{1}{4}F'^{\mu\nu}F'_{\mu\nu} - \frac{\epsilon}{2}F_{\mu\nu}F'^{\mu\nu} - y_\chi A'_\mu \bar{\chi}\gamma^\mu\chi. \quad (2)$$

The vector mediator A'_μ can also, for example, be a gauge boson from a $B-L$ symmetry, U_{B-L} [24].

- A scalar portal that includes a scalar mixing with the Higgs boson [11, 25]:

$$\mathcal{L}_{H\phi} \supset -\frac{1}{2}m_\phi^2|\phi|^2 - \kappa|H|^2|\phi|^2. \quad (3)$$

One can also have a hadrophilic or leptophilic scalar (as discussed in detail in Reference [24]) or an axion or conformal portal.

- A neutrino portal is also often considered, via the SM-neutral combination of fields LH , where L is an SM lepton doublet:

$$\mathcal{L}_N \supset LHN + gN\chi\phi + m_N NN. \quad (4)$$

We refer the reader to Reference [26] and [15] for early examples and to Reference [27] for its implementation. This portal does not typically appear in simple models for direct detection of light DM, though it is important for models of asymmetric DM, which we discuss below.

Another important feature in the hidden sector, besides its self-interactions and the portal to the visible sector, is the mass gap fixing m_χ . While by no means necessary, the theory becomes more predictive if this gap is fixed by a relation with the visible sector. This can happen, for example, if the confinement scale in the hidden sector is triggered by visible sector confinement [28] or if supersymmetry breaking in the visible sector triggers supersymmetry breaking in the hidden sector and fixes the mass scales in that sector [29]. While we do not go into the details of these models in this review, the mechanism that generates the mass gap in the hidden sector can also give rise to predictive interaction rates in terrestrial experiments; we explore some of these cases in the next two sections.

III. MECHANISMS FOR LIGHT DARK MATTER RELIC ABUNDANCE

The direct search for DM candidates whose masses are below the electroweak scale depends on the DM having couplings to the SM other than the gravitational one. The strength of those couplings, and in particular whether they are large enough to give rise to detectable signals in terrestrial experiments, is best motivated if the DM relic abundance is fixed through its interactions with the SM. We review here mechanisms for setting the relic abundance; our goal is to show how such DM candidates could be observed through a scattering or absorption process in a direct detection experiment.

A. Simplified Models in Direct Detection

Equations 2, 3 comprise simplified models of portals mediating interactions with the SM, where m_ϕ and $m_{A'}$ can be denoted more generally as mediators of mass m_M . It is often useful to employ simplified models as a general framework for understanding how relic abundance considerations interplay with astrophysical, cosmological, and direct detection constraints. A typical interaction cross section of DM with the coupling $\alpha_\chi = \frac{g_\chi^2}{4\pi}$ via a mediator, on a

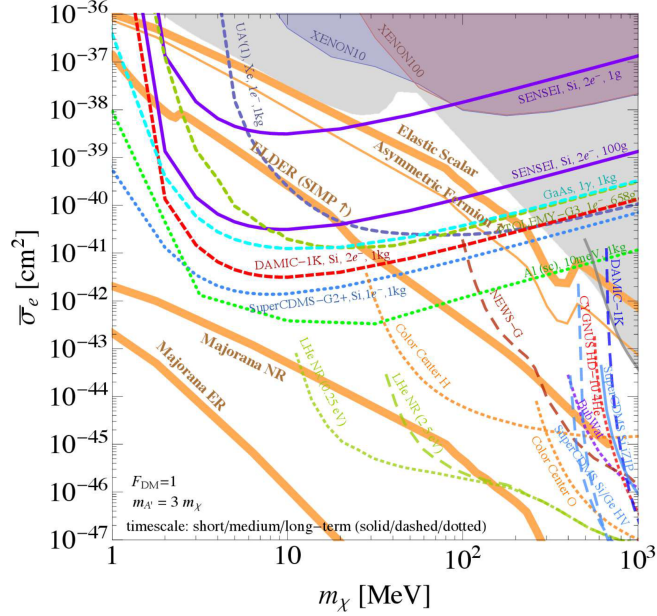


Figure 2. Direct detection cross section ($\bar{\sigma}_e$) reach for a massive vector mediator coupled to electrons as a function of DM mass (m_χ). Orange bands reflect five sets of model assumptions and correspond to the combination of couplings that fix the relic abundance through (i) P -wave freeze-out of scalar DM (elastic scalar; see discussion around Equation 13), (ii) asymmetric fermion DM (see discussion around Equation 18), or (iii) ELDERs/SIMPs (see Equation 27). These cases motivate searches by direct detection. If the DM is a Majorana fermion (Majorana NR or Majorana ER), its direct detection cross sections are suppressed and accelerator searches are better equipped for detection. Various ideas have been proposed to directly detect light DM, such as through electronic excitation in a silicon (SENSEI, DAMIC, SuperCDMS) or GaAs target, superconductors (Al SC), color centers, superfluid helium, or polar materials. Solid lines indicate a short-term timescale, dashed lines indicate a medium-term timescale, and dotted lines indicate a long-term timescale. The shaded regions indicate existing constraints. For more details regarding the experimental proposals, see Reference [8]. Abbreviations: Al SC, superconducting aluminum; DM, dark matter; ELDER, elastically decoupling relic; ER, electron recoil; HV, high voltage; NR, nuclear recoil; SIMP, strongly interacting massive particle. Figure adapted from Reference [8].

target T (electron or nucleon) having a coupling $\alpha_T = g_T^2/4\pi$, takes the form

$$\bar{\sigma}_T \equiv \frac{16\pi\alpha_T\alpha_\chi}{(m_M^2 + \mathbf{q}_0^2)^2}\mu_{T\chi}^2 \quad (5)$$

in a direct detection experiment, where $\mu_{T\chi}$ is the target-DM reduced mass and \mathbf{q}_0 is a typical momentum transfer in the experiment, used here to define the reference cross section. For electron targets, the reference momentum is taken to be $q_0 = \alpha m_e$. The same product of couplings, $\alpha_T\alpha_\chi$, typically sets the relic abundance of DM in models where DM is produced through its interaction with the SM. In the case of scattering via a heavy vector mediator on an electron target, Equation 5 with $T = e$ can be written as

$$\bar{\sigma}_e \equiv \frac{16\pi\alpha_e m_e^2}{m_\chi^4} y_{RA}, \quad (6)$$

where we have taken $m_\chi \gg m_e$ and separated a relic abundance parameter y_{RA} :

$$y_{RA} \equiv \alpha_\chi \left(\frac{m_\chi}{m_{A'}} \right)^4. \quad (7)$$

Summary plots showing the proposed reach in $\bar{\sigma}_e$ of several direct detection experiments as a function of light DM mass are shown in Figure 2 for a massive mediator and in Figure 3 for a massless mediator. In the rest of this review, one goal is to illuminate how the various reach curves and constraints are computed. The orange bands in Figure 2 and the blue band in Figure 3 correspond to the regions of model space where the DM abundance in the Universe is fixed by the same couplings that give rise to the scattering in direct detection experiments. We now turn to discussing concretely how the scattering cross section in direction detection experiments can be related to the relic abundance in three common cases that set benchmarks in terrestrial searches for light DM.

B. Thermal Freeze-Out of Symmetric Dark Matter

Thermal freeze-out occurs when the temperature drops below the DM mass and the equilibrium process, $\chi\bar{\chi} \leftrightarrow f\bar{f}$, becomes simply an annihilation process,

$$\chi\bar{\chi} \rightarrow f\bar{f}, \quad (8)$$

since the DM is too heavy to produce through the inverse process $f\bar{f} \rightarrow \chi\bar{\chi}$ when $T \ll m_\chi$. Freeze-out fixes the relic abundance to a value obtained by solving a Boltzmann equation,

$$\frac{dY_\pm}{dx} = -\frac{x\langle\sigma v\rangle s}{H(m_\chi)}(Y_+Y_- - (Y^{\text{eq}})^2), \quad (9)$$

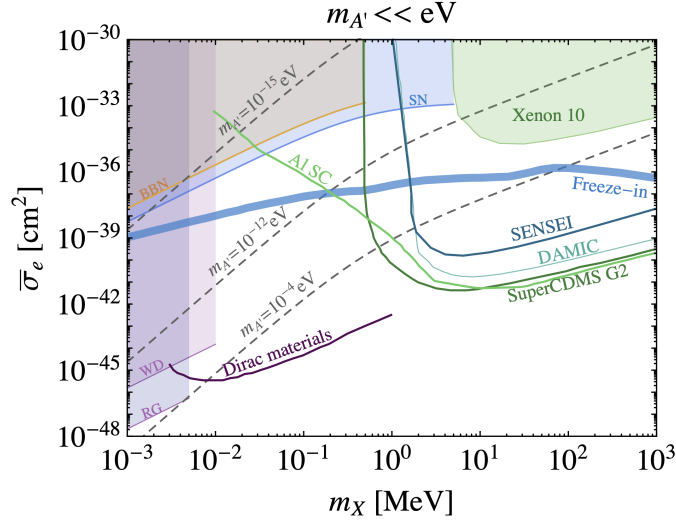


Figure 3. Direct detection cross section ($\bar{\sigma}_e$) reach for a massless dark photon mediator as a function of DM mass (m_χ). The blue band corresponds to the combination of couplings (Equation 23) where the observed relic abundance is fixed by freeze-in. Various ideas have been proposed to directly detect light DM, such as through a silicon or germanium target (SENSEI, DAMIC, SuperCDMS), superconductors (Al SC), Dirac materials, or polar materials. The shaded regions indicate constrained parameter space, such as bounds provided by stellar cooling (including RGs, WDs, and SNe) as well as by BBN. Abbreviations: Al SC, superconducting aluminum; BBN, big bang nucleosynthesis; DM, dark matter; RG, red giant; SN, supernova; WD, white dwarf. Figure adapted from Reference [24].

where we are allowing DM to have separate number densities for particle and antiparticle to permit a DM asymmetry, and $Y_\pm = n_\pm/s$, where s is the entropy density. Here $x = m_\chi/T$ is a measure of temperature (or time), the Hubble parameter $H(m_\chi)$ is evaluated at $T = m_\chi$ in a radiation-dominated universe, and $Y^{\text{eq}} \simeq ax^{3/2}e^{-x}$ is the equilibrium number density, with a dependent on the number of thermalized degrees of freedom. The annihilation cross section is parameterized as S-wave ($n = 0$) or P-wave ($n = 1$): $\langle\sigma v\rangle \equiv \sigma_0(T/m)^n = \sigma_0 x^{-n}$, where $\frac{3}{2}T = \frac{1}{2}m\langle v^2\rangle$. Note that for P-wave interactions, since the DM velocity drops as the Universe cools, the interaction rate is much smaller in the late Universe than in the early. This can be important for understanding constraints on the annihilation cross section from later epochs—for example, from the CMB at a temperature of approximately 1 eV. In the case where there

is no DM particle–antiparticle asymmetry, freeze-out occurs when $n_\chi \langle \sigma_A |v| \rangle \simeq H(x_f)$, and one can do a back-of-the-envelope calculation of the needed annihilation cross section to fix the observed relic abundance ρ_χ^0 :

$$\begin{aligned} \langle \sigma v \rangle &\sim \frac{T_f^2}{M_{\text{Pl}}} \frac{m_\chi}{\rho_\chi(T_f)} \\ &= \frac{T_f^2}{M_{\text{Pl}}} \frac{m_\chi T_0^3}{\rho_\chi^0 T_f^3} \\ &= \frac{T_0^3}{M_{\text{Pl}}} \frac{x_f}{\rho_\chi^0} \\ &\simeq 3 \times 10^{-26} \text{ cm}^3 \text{ s}^{-1} \left(\frac{x_f}{20} \right), \end{aligned} \tag{10}$$

where $x_f \simeq 20$ is the freeze-out temperature obtained from solving the Boltzmann equation for S-wave annihilation and DM in the WIMP window $m_\chi \simeq 1$ TeV. It has only logarithmic sensitivity to the DM mass. An S-wave annihilation process to a light vector particle scales parametrically as

$$\langle \sigma v \rangle \simeq \frac{\pi \alpha_\chi^2}{m_\chi^2} \sqrt{1 - \left(\frac{m_M}{m_\chi} \right)^2} \simeq 3 \times 10^{-26} \frac{\text{cm}^3}{\text{s}} \left(\frac{g_\chi}{0.4} \right)^4 \left(\frac{2 \text{ TeV}}{m_\chi} \right)^2, \tag{11}$$

where we have taken the vector force mass to be much smaller than the DM mass, $m_M \ll m_\chi$. The fact that $g_\chi \sim 1$ when $m_\chi \sim 1$ TeV is parametrically the reason that weak-scale DM is said to be motivated by thermal freeze-out, a statement known colloquially as the WIMP miracle.

One can see immediately that the DM cannot be pushed much heavier than ~ 10 TeV without running into a regime where couplings become non-perturbative and the theory is inconsistent. However, as DM becomes lighter, one simply needs to scale down the coupling product α_χ linearly with m_χ to satisfy the same relic abundance considerations. Thus, HSDM of a low mass is equally well motivated by thermal freeze-out considerations.

More generally, for an s -channel annihilation process to electrons through a mediator, vector or scalar, the annihilation cross sections at freeze-out are

$$\langle \sigma v \rangle_V \simeq \frac{16\pi \alpha_\chi \alpha_e m_\chi^2}{(4m_\chi^2 - m_{A'}^2)^2} \quad \text{and} \quad \langle \sigma v \rangle_S \simeq \frac{2\pi \alpha_\chi \alpha_e m_\chi^2}{(4m_\chi^2 - m_S^2)^2} \frac{1}{x_f}. \tag{12}$$

As DM drops below approximately 10 GeV down to $2m_e$, its relic number density remains high enough that S-wave annihilation to SM states—in the absence of a particle–antiparticle

asymmetry—during the CMB epoch is ruled out (see Reference [30–33] and discussion in Section IV B). The basic reason for the CMB constraint is that the energy released in DM annihilation can distort the surface of last scattering, placing a lower bound on the DM mass. This can be ameliorated through P-wave annihilation (which occurs if fermionic DM annihilates through a scalar mediator, or if scalar DM annihilates through a vector boson as was proposed for MeV DM; see Reference [12, 34, 35]). In this case, the annihilation rate is suppressed by the velocity of the DM in the late Universe (in the Milky Way, $v \sim 10^{-3}$, while for the smooth background, $v \sim \sqrt{T/m_\chi}$), whereas in the early Universe (at freeze-out, the velocity is $v \sim \frac{1}{3}$) the rate is similar to the S-wave case. For the S-wave case, one finds the relic abundance parameter in Equation 7, which enters into the direct detection cross section from Equation 6 as follows:

$$y_{\text{RA}} \simeq 10^{-11} \left(\frac{m_\chi}{10 \text{ MeV}} \right)^2 \left(\frac{x_f}{20} \right) \left(1 - \frac{4m_\chi^2}{m_{A'}^2} \right)^2. \quad (13)$$

For the case of P-wave annihilation through a scalar mediator, the couplings must be correspondingly (somewhat) larger to compensate the v^2 suppression. The model space of P-wave annihilating scalar DM is shown as the orange band labeled “elastic scalar” in Figure 2.

C. Thermal Freeze-Out of Asymmetric Dark Matter

The DM may also have a particle–antiparticle asymmetry that fixes the dominant component of the relic abundance, similar to what occurs for the baryons in the visible sector (for a review, see Reference [15]). However, the particle–antiparticle asymmetry of asymmetric DM becomes visible only if the symmetric abundance is efficiently removed through annihilation in the early Universe. Stated another way, symmetric freeze-out can be obtained as a limit of the more general case of asymmetric freeze-out. This is similar to the case of baryons and leptons in the SM, which efficiently annihilate through, for instance, $e^+e^- \rightarrow \gamma\gamma$ and $p\bar{p} \rightarrow \pi^+\pi^-$. In the SM, these processes are highly efficient, such that positrons, antiprotons, and neutrons are extremely rare in the Universe unless they are produced in astrophysical accelerators that generate cosmic rays. For asymmetric DM to satisfy bounds on DM annihilation rates at the CMB epoch (discussed below in Section IV B), the particle–antiparticle annihilation rate must have been large enough to effectively remove the anti-particle, placing

a lower bound on the annihilation cross section. This in turn places a lower bound on the scattering cross section via Equation 6 which also serves as a benchmark for light DM direct detection experiments. Here we briefly summarize the treatment in Reference [32] relevant for our purposes.

Solving the Boltzmann equation for a general particle–antiparticle asymmetry gives rise to the late-time ratio of particle–antiparticle asymmetries [32, 36]:

$$r_\infty \equiv \frac{Y_-}{Y_+}(\infty) \simeq \frac{Y_-(x_f)}{Y_+(x_f)} \exp\left(\frac{-\eta_\chi \lambda \sqrt{g_*}}{x_f^{n+1}(n+1)}\right), \quad (14)$$

where $\eta_\chi \equiv Y_\chi - Y_{\bar{\chi}}$ and $\lambda \equiv 0.265 M_{\text{Pl}} m_\chi \sigma_0$. It turns out that numerically one can set $Y_-(x_f)/Y_+(x_f) \sim 1$ to obtain r_∞ . The required annihilation cross section to achieve a particle-symmetric component r_∞ ($r_\infty \ll 1$ corresponds to a large asymmetry) is thus

$$\langle \sigma v \rangle \simeq c_f \times 5 \times 10^{-26} \text{ cm}^3 \text{ s}^{-1} \times \ln\left(\frac{1}{r_\infty}\right), \quad (15)$$

where $c_f \equiv \left(\frac{x_f}{20}\right) \left(\frac{4}{\sqrt{g_{*,f}}}\right)$. One can combine this with the bound on the annihilation cross section from the CMB [30–33],

$$\langle \sigma v \rangle_{\text{CMB}} \lesssim \frac{10^{-27} \text{ cm}^3 \text{ s}^{-1}}{f} \left(\frac{m_\chi}{1 \text{ GeV}}\right) \left(\frac{1}{r_\infty}\right), \quad (16)$$

to obtain an upper bound on r_∞ ,

$$r_\infty \ln\left(\frac{1}{r_\infty}\right) \lesssim \frac{0.02}{f c_f} \left(\frac{m_\chi}{1 \text{ GeV}}\right), \quad (17)$$

where f parameterizes an ionizing efficiency ($f \sim 1$ for annihilation to charged leptons but is smaller for annihilation to hadronic states). This corresponds to a lower bound on the S-wave annihilation $\langle \sigma v \rangle_{\text{CMB}} = \langle \sigma v \rangle_V$ [32]:

$$\langle \sigma v \rangle \gtrsim 5 c_f \times 10^{-26} \frac{\text{cm}^3}{\text{s}} \left(\ln\left(40 f c_f \times \frac{1 \text{ GeV}}{m_\chi}\right) + \ln \ln\left(40 f c_f \frac{1 \text{ GeV}}{m_\chi}\right) \right). \quad (18)$$

This S-wave annihilation cross section is a factor of several larger than what is required to fix the relic abundance in the symmetric S-wave case to achieve a sufficient depletion of the symmetric relic abundance (see figure 2 in Reference [32]). The CMB bound thus gives rise to a scattering cross section for the asymmetric fermion shown in Figure 2,

$$\sigma_e \gtrsim 4 \times 10^{-39} \text{ cm}^2 \left(\frac{10 \text{ MeV}}{m_\chi}\right)^2 \left(\frac{\mu_{e\chi}}{0.5 \text{ MeV}}\right)^2 \ln\left(\frac{40 \text{ GeV}}{m_\chi}\right) \frac{(4m_\chi^2 - m_M^2)^2}{m_M^4}, \quad (19)$$

which is derived by combining Equations 5, 12, and 18 for the vector mediator. The upward arrow to the right of the “asymmetric fermion” label in Figure 2 indicates that the CMB bound demands minimum couplings to remove the symmetric abundance. An elastic scalar DM line is found nearby in Figure 2 since this case requires similar, but slightly larger, couplings.

D. Freeze-In

Freeze-in is a process that dominantly occurs at low temperatures when the interactions between the hidden sector and the SM are not strong enough to bring DM into equilibrium with the SM [37]. An initially unpopulated DM state is gradually populated through occasional annihilations of SM states to DM. For example, if DM is lighter than the pion mass, the dominant freeze-in process is via electrons or plasmons (γ^*):

$$e^+e^- \rightarrow \chi\bar{\chi} \quad \text{or} \quad \gamma^* \rightarrow \chi\bar{\chi}. \quad (20)$$

For the purposes of the estimate here, we focus on the first process, though the second one affects the expected scattering rate in direct detection by up to a factor of 10 for $m_\chi \sim \text{keV}$ while having little impact for $m_\chi \sim \text{MeV}$ [38]. In the case that the DM is not initially in thermal equilibrium, the Boltzmann equation becomes

$$\frac{dY}{dT} = -\frac{\langle\sigma|v|\rangle}{HTs}n^2. \quad (21)$$

If we take $\langle\sigma|v|\rangle \sim \frac{g_\chi^2 g_e^2}{4\pi T^2}$ as expected for infrared-dominated effects, one finds the following [38, 39]:

$$Y \sim 10^{-4} \frac{g_\chi^2 g_e^2 M_{\text{Pl}}}{T}. \quad (22)$$

Taking $T \sim 1 \text{ MeV}$, where the electrons themselves drop out of thermal equilibrium, and fixing Y by the observed abundance through the relation $\rho_\chi^0 = m_\chi Y s_0$, where s_0 is the entropy density today, we obtain the approximate scaling

$$g_\chi g_e \sim 10^{-12} \sqrt{\frac{1 \text{ MeV}}{m_\chi}}, \quad (23)$$

where the number density of DM Y scales as $1/m_\chi$ in solving for the couplings. For $m_\chi \lesssim m_e$, the direct detection cross section, using Equation 5, then scales as

$$\sigma_e \simeq 10^{-39} \text{ cm}^2 \left(\frac{m_\chi}{1 \text{ keV}} \right). \quad (24)$$

This estimate corresponds to the blue band labeled “freeze-in” in Figure 3 for $m_\chi \lesssim 1 \text{ MeV}$. For $m_\chi \gtrsim m_e$, the freeze-in temperature in Equation 22 is $T \sim m_\chi$, and the scattering cross section becomes approximately independent of m_χ . At even higher masses ($m_\chi \gtrsim m_\pi$), new processes involving pions enter; we do not estimate this rate here. One can see, however, that over much of the mass space, simple estimates allow one to obtain an approximate expected interaction cross section with electrons.

E. Strongly Interacting Massive Particles and Elastically Decoupling Relics

DM freeze-out can be dominated by $3 \rightarrow 2$ processes [21, 40] with a “cross section” parameterized by

$$\langle \sigma_{3 \rightarrow 2} v^2 \rangle \equiv \frac{\alpha^3}{m_\chi^5}. \quad (25)$$

(Note that this cross section does not carry the usual dimensions, but is defined so that $\Gamma_{3 \rightarrow 2} = n_\chi^2 \langle \sigma_{3 \rightarrow 2} v^2 \rangle$ gives a rate.) Parametrically α is proportionate to a dark gauge coupling constant $\alpha_D \equiv g_D^2/4\pi$, though here, following References [40], [21], and [41], α is allowed to absorb $\mathcal{O}(1)$ factors. The observed relic abundance is obtained when

$$\alpha \simeq 0.3 \left(\frac{m_\chi}{10 \text{ MeV}} \right). \quad (26)$$

These processes continually dump kinetic energy into the DM by cannibalizing the DM’s rest energy. This is observationally ruled out since the DM would be much warmer than observed [42, 43]. The solution to this problem, as proposed in References [40] and [21], is to have a light mediator that bleeds off the energy into the SM sector continuously, typically via a kinetic mixing parameter ϵ between a dark photon and a visible one. In this picture, the elastic scattering process that bleeds off the excess energy decouples after the freeze-out of the $3 \rightarrow 2$ process.

This idea was generalized in References [44] and [41] by allowing $3 \rightarrow 2$ processes in the hidden sector as well as $2 \rightarrow 2$ processes (notably $\chi\bar{\chi} \rightarrow e^+e^-$) as in freeze-out to play a role.

Since the $\chi\bar{\chi} \leftrightarrow e^+e^-$ decouples when both directions are in equilibrium, this was called an elastically decoupling relic (ELDER) [41, 44]. Thus, the ELDER smoothly interpolates between the elastic freeze-out case (for large enough kinetic mixing, where the $3 \rightarrow 2$ process freezes out well before the annihilation to SM) and the SIMP case (where elastic decoupling with the SM occurs before the $3 \rightarrow 2$ process freezes out). In the ELDER limit, the relic abundance is set dominantly by the decoupling temperature from the SM, which is given by the following [41]

$$y_{\text{ELDER}} = \epsilon^2 \alpha_D \left(\frac{m_\chi}{m_{A'}} \right)^4 \simeq 6 \times 10^{-15} \left(\frac{g_{*,d}}{10} \right)^{1/2} \left(\frac{m_\chi}{10} \right) \left(\frac{x_d}{17} \right)^6, \quad (27)$$

where ϵ and α_D are defined above, and $x_d = m_\chi/T_d$ with T_d denoting the elastic decoupling temperature. This allows one to give a precise benchmark for the ELDER scenario (see the orange band labeled ELDER (SIMP \uparrow) in Figure 2).

IV. ASTROPHYSICAL, COSMOLOGICAL, AND ACCELERATOR PROBES

When considering whether a DM candidate of a very low mass is detectable in a terrestrial experiment, a wide range of astrophysical, cosmological, and collider constraints must be taken into consideration. Here we summarize the main features; for further discussion regarding the interplay of the constraints with terrestrial observations, we refer the reader to References [32], [16], and [24].

A. Big Bang Nucleosynthesis

BBN is a powerful constraint if the DM is lighter than an MeV in mass. Measurements of hydrogen, deuterium, and helium—synthesized dominantly when the Universe had a temperature $T_{\text{BBN}} \sim 0.1\text{--}1$ MeV at a time $t \sim 1$ s—indicate that the Universe was expanding at a rate consistent with a relativistic SM photon and three neutrino species. If any other state were in equilibrium with the SM (*e.g.*, through $\chi\bar{\chi} \leftrightarrow f\bar{f}$ interactions), this would cause the Universe to expand more quickly and would change the relative abundance of the light elements, parameterized by the effective number of neutrino species, N_{eff} . Current data constrain $\Delta N_{\text{eff}}^{\text{BBN}} \lesssim 0.2$ [45, 46], implying a more than 3σ tension with a single real scalar

having a temperature similar to that of neutrinos. This implies that any DM candidate with a mass $\lesssim 10$ MeV has its couplings to the SM constrained by BBN.

Note that in general, for a DM candidate to be detectable, we must consider not only the DM degrees of freedom but also the mediator that couples the DM to the SM. The mediator must also either (a) be heavier than ~ 1 – 10 MeV, (b) have sufficiently small couplings to the SM that it remains out of equilibrium, or (c) contribute $\Delta N_{\text{eff}}^{\text{BBN}} \gtrsim 0.57$ (for a real scalar DM) and be in $\sim 4\sigma$ tension with BBN. This limits the types of DM models that can be detected in terrestrial experiments (for an extensive discussion and application to terrestrial experiments, see Reference [24]; for updated BBN constraints, see References [45] and [46]).

For example, BBN constraints are the reason why, for the model space detectable by terrestrial direct detection experiments, DM lighter than an MeV should be mediated by a very light particle. Direct detection experiments are sensitive to extremely small couplings via light mediators (as in Equation 23) because of the direct detection enhancement at low momentum transfers (as in Equation 5 with $m_M \rightarrow 0$). For such small couplings, the hidden sector is not in equilibrium with the visible sector except at larger couplings (see the shaded orange region in Figure 3). Likewise, for DM mediated through a heavier particle (having mass $m_M \gtrsim m_\chi v$, where v is the Milky Way virial velocity), the couplings are much larger (see, *e.g.*, Equation 11 for typical freeze-out couplings). In this case, the hidden sector generically comes into equilibrium with the visible sector, such that hidden sectors with masses below a few MeV are already ruled out by BBN; this is one reason that the range of the plot in Figure 2 extends only to $m_\chi \gtrsim 1$ MeV.

B. Cosmic Microwave Background

As discussed above in Sections III B and III C, the CMB places a variety of constraints on a DM candidate of a very low mass. First, the CMB also places a constraint, at 2σ , roughly consistent with the BBN bound, $\Delta N_{\text{eff}}^{\text{CMB}} \lesssim 0.6$. Since the CMB epoch is at a redshift $z \sim 10^3$ – 10^4 , while the BBN epoch is at $z \sim 10^{10}$, one cannot simply assume that if the constraint on additional thermal relativistic species is met at one epoch, it is also met at a different epoch. Note that in the future, CMB Stage IV will dramatically improve on this constraint, $\sigma(N_{\text{eff}}^{\text{CMB}}) \approx 0.03$ [46].

In addition, the CMB is very sensitive to any additional ionizing radiation that can be dumped into the photon–baryon bath. For example, the Planck limit on DM energy injection due to annihilation is given by Equation 18. Since, to set the thermal relic abundance for DM through annihilation, we require $\langle\sigma v\rangle \sim 3 \times 10^{-26} \text{ cm}^3 \text{ s}^{-1}$, this implies that light (sub-GeV) DM cannot have its relic abundance set by S-wave annihilation while remaining consistent with CMB-epoch ionization constraints. There are two ways to circumvent this constraint, as discussed in Section III B: P-wave annihilation where the cross section is v suppressed, or asymmetric DM where $r_\infty \ll 1$. As highlighted above, models of asymmetric DM must have an efficient mechanism for removing the symmetric abundance of DM early in the Universe. This implies a lower bound on the annihilation cross section in the early Universe (shown in Figure 2 as the asymmetric fermion curve) to adequately dilute the symmetric abundance.

C. Large-Scale Structure

Large-scale structure places two important bounds on DM having a very low mass. The first important bound is the warm DM bound, from the formation of structure on small scales, as observed with Lyman- α forest and other large-scale structure measurements of DM clustering [9, 47]. Thermalized DM has the following relation between its velocity and temperature:

$$v = \sqrt{\frac{3T}{m_\chi}}. \quad (28)$$

If DM has its temperature on the same order as the visible temperature $T \sim 10^{-4} \text{ eV}$, and we require DM to be cold enough for it to fall into structures having virial velocity $v \sim 10^{-4}$ (*e.g.*, as observed in dwarf galaxies), this implies that DM should have the following mass:

$$m_\chi \gtrsim 10 \text{ keV}. \quad (29)$$

This is the back-of-the-envelope estimate of the warm DM bound (which can be more carefully derived by simulating the formation of structures with warm DM; see, *e.g.*, References [9] and [47]). DM may still be lighter than this bound, but its temperature should not be set by the interactions with the SM (*e.g.*, as happens with non-thermal mechanisms such as the misalignment mechanism for the axion or inflationary production of vector DM) [48, 49].

If DM has an interaction with the SM through a relatively light gauge boson, this can also cause late kinetic decoupling between the SM and the dark sector and modify the matter power spectrum on small scales. For example, DM can couple to neutrinos through a mediator (product of couplings to the mediator $g_\chi g_\nu$), giving rise to a kinetic decoupling temperature:

$$T_{\text{kd}} \simeq \text{keV} \frac{m_M}{\text{MeV}} \left(\frac{m_\chi}{\text{MeV}} \right)^{1/4} \left(\frac{10^{-6}}{g_\chi g_\nu} \right)^{1/2}. \quad (30)$$

Such a kinetic decoupling temperature is bounded by the Lyman- α forest (see Reference [35]).

DM of a very low mass also tends to come with new light forces that can mediate large self-interactions. The self-interaction rate is bounded by the shape of DM halos, which implies that DM self-interactions should be rare enough that the formation of halos is dominated by gravitational interactions. This implies the following [50]:

$$\frac{\sigma}{m_\chi} \lesssim 0.1\text{--}10 \text{ cm}^2 \text{ g}^{-1}, \quad (31)$$

where the large range of possible bounded cross sections is due to the large range of system mass scales and interaction times (from dwarf galaxies at $10^7 M_\odot$ to clusters of galaxies at $10^{15} M_\odot$) as well as the still-somewhat-imprecise nature of simulations, which depends on baryonic effects and their (non-linear) feedback on the DM structure formation process. Especially when the mediator is light, this places severe limits on the DM–mediator coupling (taking $\frac{\sigma}{m_\chi} = 1 \text{ cm}^2 \text{ g}^{-1}$):

$$\alpha_\chi \lesssim 6 \times 10^{-10} \times \left(\frac{m_\chi}{1 \text{ MeV}} \right)^{3/2}. \quad (32)$$

When the mediator becomes massive ($m_\phi > m_\chi v$), we have a less severe limit:

$$\alpha_\chi \lesssim 0.025 \left(\frac{1 \text{ keV}}{m_\chi} \right)^{1/2} \left(\frac{m_\phi}{1 \text{ MeV}} \right)^2. \quad (33)$$

For further discussion, we refer the reader to References [51] and [52].

D. Stellar Evolution and Cooling

When the DM, or the mediator, is lighter than the temperature of a star, production of dark-sector particles can lead to cooling that is more efficient than what happens in the

SM, where states are strongly coupled to the stellar plasma (for a classic review, see Reference [53]). This cooling changes the evolution of the star from that predicted by standard theory, and it could be observed. This has long been appreciated in particular for axions, but it also becomes relevant for DM and mediators with masses $\lesssim 30$ MeV, the temperature of a supernova. In addition to supernovae, red giants (RGs; relevant for masses $\lesssim 10$ keV), horizontal branch stars (HBs; $\lesssim 100$ keV) for nucleon couplings, and white dwarves (WDs; $\lesssim 10$ keV) are all relevant. Constraints from these stellar cooling limits are shown as shaded regions in Figure 3 and 4. When the coupling becomes large enough, particularly in dense environments like the neutron stars that form inside supernovae, trapping becomes relevant. The supernova cooling bounds have recently been updated in Reference [54], while the RG, HB, and WD stellar cooling bounds for mediator couplings to nucleons, electrons, and dark photons are quoted in detail in Reference [24].

Light DM, especially if it carries a particle–antiparticle asymmetry that prevents annihilation, can accumulate in the centers of stars and also cause a change in their evolution. This has been considered in particular for neutron stars, either due to inducing an instability (for a summary, see the discussion in Reference [16]) or due to kinetic heating [55]. Accumulation of light DM can also lead to modification of main branch stellar evolution [56] and in brown dwarves [57] and WDs [58, 59]. For a fairly up-to-date list of references regarding compact star constraints on HSDM interactions with electrons and nucleons, we refer the reader to Reference [60].

E. Accelerator Probes of Light Hidden Sectors

Intensity experiments, such as beam dumps featuring a large number of protons on target, can probe relatively light (typically sub-GeV mass) hidden-sector particles. The constraints are most direct on the mediating particle (vector or scalar) and depend on the decay channel, whether to visible (notably e^+e^-) or invisible particles.

- Invisible decays: In the case of invisible decays, the mediator either decays dominantly to DM, or is stable on detector timescales. If the mediator couples to hadrons and is lighter than Λ_{QCD} , it can be constrained through the invisible processes $B \rightarrow K\phi$ and $K \rightarrow \pi\phi$, where ϕ is a scalar or vector mediator [24]. The effective coupling to

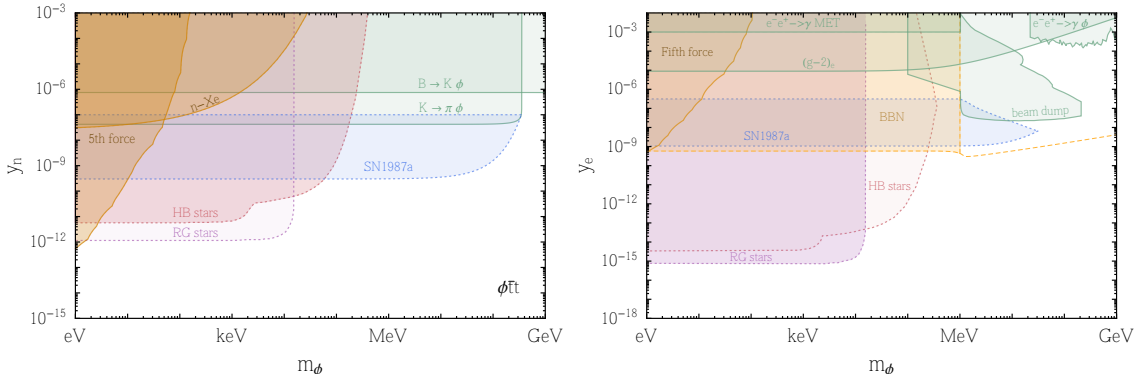


Figure 4. Constraints on (a) mediator-nucleon coupling $\mathcal{L} = y_n \phi \bar{n} n$ (mediated by a top quark) and (b) mediator-electron coupling $\mathcal{L} = y_e \bar{e} e$ as a function of the mediator mass. Abbreviations: BBN, big bang nucleosynthesis; HB, horizontal branch; MET, missing transverse energy; RG, red giant. Figure adapted from Reference [24].

nucleons constrained in this way is $y_n \lesssim 10^{-5}$ – 10^{-7} , depending on the flavor structure of the ϕ –quark coupling. If the mediator couples to electrons, it can be constrained by $e^+e^- \rightarrow \gamma\phi$, that is, a monophoton search in BaBar. The electron $(g-2)$ measurement also provides a powerful bound. For a summary of collider bounds, we refer the reader to References [61], [62], and [24].

- Visible decays: For visible decays, the constraints are strongest when the mediator is produced, and decays directly to charged leptons $\ell^+\ell^-$ [63, 64]. These constraints are typically labeled as beam-dump constraints.

While we have not exhaustively summarized the accelerator probes on light hidden sectors, these summarize the general types of constraints on mediators. We show two summary plots in Figure 4 for nucleon and lepton couplings that demonstrate the collider, stellar, and fifth-force bounds on the nucleon–scalar and electron–scalar couplings.

V. DIRECT DETECTION OF LIGHT-PARTICLE DARK MATTER

The direct detection of light DM depends on considerations of both kinematics and interactions. That is, one needs to find a target material with a strong response (i.e., Dynamic Structure Factor) for energy and momentum deposition in the DM kinematic regime for

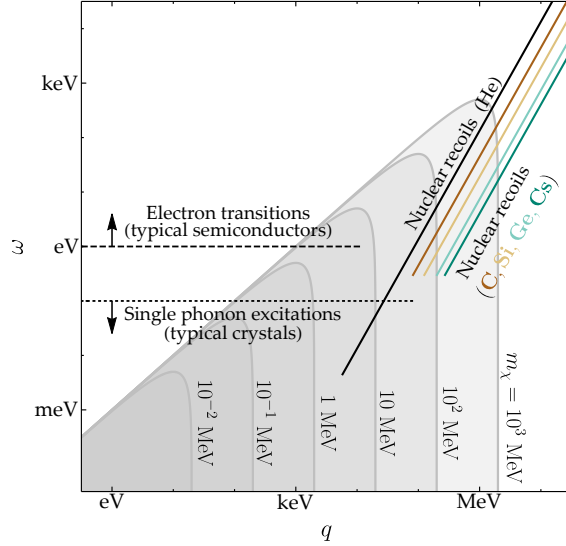


Figure 5. The kinematic parameter space of light dark matter in terms of the energy deposition (ω) and momentum transfer (q) in a direct detection experiment. The shaded parabolas correspond to the range of energy and momentum that a dark matter particle of a given mass can deposit (Equation 35). The nuclear recoil curves correspond to the energy deposit on a nucleus (Equation 37). The horizontal lines at 1 eV and 100 meV correspond to the energy gaps (as $q \rightarrow 0$) of electronic excitations (in semiconductors) and optical phonons (in crystals). Figure adapted from Reference [65].

the relevant type of interaction. We briefly summarize both before describing the particular mechanisms for detection of light DM.

In direct detection, DM must be able to cause a transition from the initial state to the final state $|i\rangle \rightarrow |f\rangle$ of the target system, with the DM typically depositing some momentum $\mathbf{q} = \mathbf{p} - \mathbf{p}'$ (where $\mathbf{p} = m_\chi \mathbf{v}$ is the initial DM momentum and \mathbf{p}' is the final DM momentum), which corresponds to some energy ω deposited by the DM on the target:

$$\omega = \frac{1}{2}m_\chi v^2 - \frac{(m_\chi \mathbf{v} - \mathbf{q})^2}{2m_\chi} = \mathbf{q} \cdot \mathbf{v} - \frac{q^2}{2m_\chi}. \quad (34)$$

Note that this expression assumes that the DM has no internal excitations (such as energy levels) that could cause the transition to be inelastic on the DM side. The energy deposited is bounded by a parabola,

$$\omega \leq qv_{\max} - q^2/2m_\chi, \quad (35)$$

as first illustrated in Reference [65] and reproduced in Figure 5. This figure shows the basic kinematic requirements of a material to allow for a detection event: The target material must have a state whose transition energy and momentum lie below (and within) the DM kinematic parabola. In addition, the closer a mode in the material is to the upper part of the parabola, the more energy can be read out, allowing in many cases for a more viable path toward detection. DM can never transfer more momentum than the following:

$$q_{\text{BW}} = 2m_{\chi}v_{\text{max}}, \quad (36)$$

which represents the “brick wall” limit at which little energy is deposited, corresponding to the right edge of the DM kinematic parabola. Take, for example, the case of nuclear recoils, where the energy deposit is

$$\omega = \frac{q^2}{2m_N}, \quad (37)$$

where m_N is the target nucleus mass, also shown in Figure 5. At the point where the nuclear recoil kinematic curve intersects the DM parabola, only a small fraction of the DM kinetic energy is deposited onto the nucleus,

$$\omega = \frac{2m_{\chi}^2v^2}{m_N} \ll \frac{m_{\chi}v^2}{2}, \quad (38)$$

when the DM is lighter than the typical SM nucleus mass. One immediately sees that sub-GeV DM is kinematically poorly matched to SM nuclei, and one should search for other targets for DM interactions. We now summarize the types of excitations that are relevant in each mass regime.

A. Targets and Excitations for Dark Matter Interactions

- For DM with mass $\gtrsim 30$ MeV, nuclear recoils are a relevant target, though they extract only a small fraction of the DM kinetic energy. Since the DM energy deposition is given in Equation 37, in order to extract the maximum energy deposition ω , the lightest target is preferable. In particular, superfluid helium has been identified as a promising target for the TESSERACT DM experiment. The lower end of the DM mass range $m_{\chi} \gtrsim 30$ MeV corresponds to a DM energy deposit on nuclei (via Equation 37) larger

than $\omega \gtrsim 500$ meV, corresponding to the typical energy of collective excitations, where the nucleus can no longer be treated as free (see discussion in Reference [65]). For smaller energy depositions, the relevant excitations are phonons.

- For DM with mass $m_\chi \gtrsim 1$ MeV and kinetic energy $\omega \gtrsim 1$ eV, electrons in targets such as semiconductors (having a typical band gap of 1 eV) and ionization in noble liquids such as xenon (with an ionization threshold of ~ 10 eV) are good targets and have been explored extensively [66–68]. Ripping an electron out of a two-dimensional material such as graphene, with a work function also in the 1-eV energy range [69] and breaking chemical bonds [70] with energy in the tens-of-eV range, has also been proposed.
- At slightly lower energy depositions, in the 100-meV range, collective excitations such as optical phonons (gapped excitations having energy ω_{ph}) become available and have been proposed as a viable pathway [52, 71], having greatest sensitivity via scattering for DM in the $m_\chi \gtrsim$ keV–MeV mass range. Collective excitations are highly sensitive to heavier DM as long as the momentum transfer is smaller than that required to kick the ion out of the lattice potential $q \lesssim \sqrt{2m_N\omega_{\text{ph}}} \sim 10$ –100 keV. This momentum corresponds to that carried by MeV mass DM in the Milky Way, though for heavier DM only a small fraction of its total momentum may be transferred, especially if the mediator is light, having a $1/q^4$ enhancement in the cross section as in Equation 5 with $m_M \rightarrow 0$ (for a detailed analysis, see Reference [71]). The SPICE (sub-eV Polar Interactions Cryogenic Experiment) experiment has research underway to detect single phonons in crystals [72]. In addition to phonons, magnons are a different type of collective excitation in materials that can detect spin-dependent DM interactions [73].
- Other gapped excitations, such as vibrational degrees of freedom in organics [74], and electronic excitations with small gaps, such as occur in superconductors [51, 75], Dirac materials [69, 76], heavy fermion materials [77], and doped semiconductors [78], are also viable targets for $m_\chi \gtrsim$ keV DM.

So far, we have explored the importance of kinematic matching between DM and target. We now examine the strength of the target response to a given energy ω and momentum

\mathbf{q} deposition. This requires computing the quantum mechanical matrix element entering into Fermi's Golden Rule for interaction rates. The matrix element in turn depends on the interaction type, such as spin-independent, spin-dependent, or a more generic interaction such as an electric or magnetic dipole or anapole. In the next sub-sections, we lay out the general quantum mechanical framework for computing the rate and then apply it to spin-independent scattering. In Section VI A, we consider more general interactions in an effective field theory (EFT) framework.

B. Quantum Mechanics of Dark Matter Scattering

The interaction type enters directly into the calculation of the matrix element for the DM to induce a transition from an initial to a final state in a target material. The DM deposits some energy and momentum (ω, \mathbf{q}) within the kinematically allowed DM parabola shown in Figure 5, and the over-arching goal is to find a material with a strong quantum mechanical response, encapsulated in a Dynamic Structure Factor. For a more complete discussion of the physics reviewed here, we refer the reader to References [65] and [79].

Quantum mechanics enters in determining the transition rate from the initial state to the final state of the target material $|i\rangle \rightarrow |f\rangle$ via a simple application of Fermi's Golden Rule:

$$\Gamma(\mathbf{v}) = V \int \frac{d^3q}{(2\pi)^3} \sum_f |\langle \mathbf{p}', f | H_{\text{int}} | \mathbf{p}, i \rangle|^2 2\pi \delta(E_f - E_i - \omega), \quad (39)$$

where H_{int} is the interaction Hamiltonian, and we assume throughout that the DM state factorizes from the target state (since they are unentangled), $|\mathbf{p}, i\rangle = |\mathbf{p}\rangle \otimes |i\rangle$, *etc.*, and V is the volume of the target. The interaction rate in Equation 39 depends on the DM velocity \mathbf{v} , whose typical value in the Milky Way galaxy is $v \sim 10^{-3}$. The detectable interaction rate, per unit of target mass, is extracted by integrating over the DM velocity phase space:

$$R = \frac{1}{\rho_T} \frac{\rho_\chi}{m_\chi} \int d^3v f_\chi(\mathbf{v}) \Gamma(\mathbf{v}), \quad (40)$$

where ρ_χ and ρ_T are the DM and target densities, and f_χ is typically taken to be a Maxwell-Boltzmann distribution truncated at the escape velocity $v_{\text{esc}} \sim 600 \text{ km s}^{-1}$ of the DM from the galaxy. Note that while $\Gamma(\mathbf{v})$ is a rate, R is a rate per unit of mass.

To illustrate the principles discussed above, we first consider DM scattering via a spin-independent interaction. The DM creates a potential,

$$\langle \mathbf{p}' | H_{\text{int}} | \mathbf{p} \rangle = V(\mathbf{q}) \quad (41)$$

to which the target responds. It is convenient to factorize this potential into a material response \mathcal{F}_T (which is agnostic about the DM) and a DM matrix element \mathcal{M} (which is agnostic about the target):

$$V(\mathbf{q}) = \mathcal{M}(q) \mathcal{F}_T(\mathbf{q}). \quad (42)$$

For spin-independent scattering, the DM-induced potential $\mathcal{M}(q)$ is characterized by a fiducial cross section and a mediator form factor:

$$\mathcal{M}(q) = \mathcal{M}(q_0) \mathcal{F}_{\text{med}}(q), \quad (43)$$

where $\mathcal{F}_{\text{med}}(q)$ is either 1 (for a heavy mediator) or $(q_0/q)^2$ (for a light mediator with momentum dependence typical of Rutherford scattering). $\mathcal{M}(q_0)$ is related to a reference cross section convenient for parameterizing the overall strength of the interaction via

$$\bar{\sigma}_T \equiv \frac{\mu_{\chi T}^2}{\pi} |\mathcal{M}_{\chi T}(q_0)|_{q_0=m_\chi v_0}^2, \quad (44)$$

where $\mu_{\chi T}$ ($T = n$ or e) denotes the DM–target (nucleon or electron) reduced mass. The target response $\mathcal{F}_T(q)$, for spin-independent interactions, is traditionally absorbed into what is known as the Dynamic Structure Factor (S), which characterizes the response of the material:

$$S(\mathbf{q}, \omega) \equiv \frac{1}{V} \sum_f |\langle f | \mathcal{F}_T(\mathbf{q}) | i \rangle|^2 2\pi \delta(E_f - E_i - \omega), \quad (45)$$

where E_f and E_i are the final and initial energies of the target. The formalism where the DM scattering rate is proportional to the Dynamic Structure Factor is valid as long as the scattering is spin-independent. Below, we will generalize the calculation to a generic type of potential, including spins; however, for intuition, and to match to the standard condensed matter understanding, we start with the spin-independent case. The DM–target scattering rate can thus be written in a unified way in terms of the Dynamic Structure Factor:

$$\Gamma(\mathbf{v}) = \frac{\pi \bar{\sigma}}{\mu^2} \int \frac{d^3 q}{(2\pi)^3} \mathcal{F}_{\text{med}}^2(q) S(\mathbf{q}, \omega). \quad (46)$$

The three basic types of spin-independent interactions considered—nuclear recoil, electron excitation, and phonon excitation—can be expressed in terms of the Dynamic Structure Factor. As shown below, we can reproduce the results in the literature using this simple unifying language. The Dynamic Structure Factor is a material-specific response that depends kinematically only on the input (\mathbf{q}, ω) provided by the DM interaction. The Dynamic Structure Factor can be generalized from spin-independent interactions within an EFT framework but using the same basic tools introduced here. We take on that task in the next section, but first we summarize the broad types of interactions used for light DM detection—nuclear recoil, electronic excitations, and single phonon excitation—in the language of the Dynamic Structure Factor.

1. Nuclear recoils

In the case of nuclear recoils, for each species of nucleus, the Dynamic Structure Factor is

$$S(\mathbf{q}, \omega) = 2\pi \frac{\rho_T}{m_N} \frac{f_N^2}{f_n^2} F_N^2(q) \delta\left(\frac{q^2}{2m_N} - \omega\right), \quad (47)$$

where m_N is the target nucleus mass, $F_N(q)$ is the nuclear form factor (often taken to be the Helm form factor), f_N is the coupling to the nucleus, and f_n is the coupling to a nucleon which we divide through by convention to cancel the same coupling in the cross section (Equation 44). Note that a single nucleus response is appropriate as long as the nucleus can be treated as free. This occurs when the energy deposition is greater than a typical phonon energy, $\omega \gg \omega_{\text{ph}} \simeq 10\text{--}500$ meV (or, equivalently, $q \gg \sqrt{m_N \omega_{\text{ph}}}$).

2. Electronic excitations

At the next level of complexity and at lower energy depositions and momentum transfer, DM interactions can induce electronic transitions. In this case, the Dynamic Structure Factor depends on the electron wavefunctions in the initial and final states:

$$S(\mathbf{q}, \omega) = \frac{2\pi}{V} \left(\frac{f_e}{f_e^0}\right)^2 \sum_{i,f} \delta(E_f - E_i - \omega) \left| \int \frac{d^3 k'}{(2\pi)^3} \frac{d^3 k}{(2\pi)^3} (2\pi)^3 \delta^3(\mathbf{k}' - \mathbf{k} - \mathbf{q}) \psi_f^*(\mathbf{k}') \psi_i(\mathbf{k}) \right|^2,$$

where the sum over i and f is over all the initial and final electronic states whose energy difference is $\omega = E_f - E_i$. In a semiconductor, the relevant states are core, valence, conduction, and free electrons, where the wavefunctions are written in terms of Bloch waves labeled by a band index I and wavenumber \mathbf{k}_1 :

$$\psi_{I,\mathbf{k}_1}(\mathbf{x}) = \frac{1}{\sqrt{V}} \sum_{\mathbf{G}_1} u_I(\mathbf{k}_1 + \mathbf{G}_1) e^{i(\mathbf{k}_1 + \mathbf{G}_1) \cdot \mathbf{x}}, \quad (48)$$

$$\psi_{I,\mathbf{k}_1}(\mathbf{k}) = \int d^3x \psi_{I,\mathbf{k}_1}(\mathbf{x}) e^{-i\mathbf{k} \cdot \mathbf{x}} = \frac{1}{\sqrt{V}} \sum_{\mathbf{G}_1} u_I(\mathbf{k}_1 + \mathbf{G}_1) (2\pi)^3 \delta^3(\mathbf{k}_1 + \mathbf{G}_1 - \mathbf{k}) \quad (49)$$

where \mathbf{G}_1 is a reciprocal lattice vector (Umklapp). This immediately leads to a Dynamic Structure Factor,

$$S(\mathbf{q}, \omega) = \frac{2}{V} \sum_{i,f} \int_{1\text{BZ}} \frac{d^3k_1}{(2\pi)^3} \frac{d^3k_2}{(2\pi)^3} 2\pi \delta(E_{f,\mathbf{k}_2} - E_{i,\mathbf{k}_1} - \omega) \times \left| \sum_{\mathbf{G}_1, \mathbf{G}_2} (2\pi)^3 \delta^3(\mathbf{k}_2 + \mathbf{G}_2 - \mathbf{k}_1 - \mathbf{G}_1 - \mathbf{q}) u_f^*(\mathbf{k}_2 + \mathbf{G}_2) u_i(\mathbf{k}_1 + \mathbf{G}_1) \right|^2, \quad (50)$$

where the prefactor of 2 comes from summing over degenerate spins. Now we can define a crystal form factor with an Umklapp \mathbf{G} , which lets us take into account in momentum space the periodicity of the crystal lattice,

$$f_{[i,\mathbf{k}_1,f,\mathbf{k}_2,\mathbf{G}]} \equiv \sum_{\mathbf{G}_1, \mathbf{G}_2} u_f^*(\mathbf{k}_2 + \mathbf{G}_2) u_i(\mathbf{k}_1 + \mathbf{G}_1) \delta_{\mathbf{G}_2 - \mathbf{G}_1, \mathbf{G}}, \quad (51)$$

so that we can rewrite the Dynamic Structure Factor as follows:

$$S(\mathbf{q}, \omega) = \frac{2}{V} \sum_{i,f} \int_{1\text{BZ}} \frac{d^3k_1}{(2\pi)^3} \frac{d^3k_2}{(2\pi)^3} 2\pi \delta(E_{f,\mathbf{k}_2} - E_{i,\mathbf{k}_1} - \omega) \times \sum_{\mathbf{G}} (2\pi)^3 \delta^3(\mathbf{k}_2 - \mathbf{k}_1 - \mathbf{G} - \mathbf{q}) |f_{[i,\mathbf{k}_1,f,\mathbf{k}_2,\mathbf{G}]}|^2. \quad (52)$$

This formula can also be applied to the case of superconductors, where the calculation is relatively simple because, for energy depositions well above the Cooper pair binding energy, the electrons behave as free particles in a Fermi-degenerate sea. In that case, $\mathbf{G} = 0$ and the crystal form factor is simply replaced by the Fermi-Dirac distributions,

$$|f_{[i,\mathbf{k}_1,f,\mathbf{k}_2,\mathbf{G}]}|^2 = f(\omega_{k_1})(1 - f(\omega_{k_2})), \quad (53)$$

where $f(E_i) = [1 + \exp(\frac{E_i - \mu_i}{T})]^{-1}$ is the Fermi–Dirac distribution of electrons at temperature T . In the limit $T \rightarrow 0$, the Dynamic Structure Factor reduces to the following [51]:

$$S(\omega, \mathbf{q}) \simeq \frac{m_e^2 \omega}{\pi q} \Theta(qv_F - \omega), \quad (54)$$

where $v_F \simeq 10^{-2}$ is the Fermi velocity of electrons in a superconductor.

The technical obstruction to computing DM interaction rates in materials like semiconductors is knowledge of the electronic wavefunctions. In some cases, especially where the electrons are more tightly bound [80], analytic atomic wavefunctions can provide an approximation that gives correct order-of-magnitude estimates for DM interaction rates [81, 82]. However, especially for conduction electrons, these approximations are not very good. There now exist multiple codes to compute spin-independent scattering rates of light DM electrons using wavefunctions computed via density functional theory (DFT). This includes the QEDARK [68], QCDARK [83], EXCEED-DM [80, 84], and DARKELF [85] packages. EXCEED-DM extended QEDARK by including the all-electron reconstructed wavefunctions and additional electronic states outside of valence and conduction bands. DARKELF makes use of the DFT-computed dielectric function $\epsilon(\omega, \mathbf{q})$ with the observation that the dynamic structure function, *for dark photon-like scattering on electrons*, can be written in the low-temperature limit as follows [77, 86]:

$$S(\omega, \mathbf{q}) = \frac{q^2}{2\pi\alpha_{em}} \text{Im} \left[\frac{-1}{\epsilon_L(\omega, \mathbf{q})} \right]. \quad (55)$$

This can be a convenient expression for spin-independent scattering if the dielectric function is available for all (ω, \mathbf{q}) of interest.

Table I summarizes the types of targets, and their gaps, proposed for DM interacting with the electron. There are already many experiments in progress that realize these ideas:

- Ionization in atoms and excitation across the band gap in semiconductors were the first processes proposed to detect MeV–GeV DM and are currently being implemented in semiconductor targets in the SuperCDMS, SENSEI, DAMIC, and EDELWEISS experiments. The Xenon (PandaX, Xenon1T, LUX) and liquid argon (DarkSide) experiments have also done searches for ionization of electrons.
- Cooper pair breaking in superconductors has been implemented to search for keV–GeV light DM with superconducting nanowires [87].

Target	Reaction processes	Typical gap	Elastic or inelastic?	DM Mass Range
Atom	Ionization	10 eV	Inelastic	$\gtrsim 10$ MeV–GeV
Semiconductor	Excitation across band gap	~ 1 eV	Inelastic	MeV–GeV
Superconductor	Cooper pair breaking	~ 1 meV	Approximately elastic ^a	$\gtrsim 1$ keV–GeV
Graphene	Electron ejection	~ 1 eV	Inelastic	$\gtrsim 1$ MeV–GeV
Dirac material	Excitation across band gap	~ 0 –1 meV	Inelastic	keV–GeV
Heavy fermion material	Excitation across band gap	~ 10 meV	Inelastic	10 keV–GeV

^a The superconductor DM detection process is elastic for energy depositions well above the Cooper pair binding energy.

Table I. Summary of the target materials that have been proposed for dark matter (DM) detection through electron excitation.

For a currently complete discussion of the ongoing experimental efforts, which we do not attempt to cite in detail here, we refer the reader to Reference [88] (especially Figure 1).

3. *Single Phonon excitations*

When the energy deposition drops below $\omega \sim 100$ meV $\sim q^2/2m_N$, with $q \sim 10$ –100 keV, the nucleus can no longer be treated as free and the relevant degrees of freedom are no longer single ions. Phonons are collective oscillations of atoms in fluids (such as superfluid helium) or crystals (including metals like superconductors). For a crystal with a lattice structure having n ions in a unit cell, there are $3n$ such modes. Three of those modes are gapless acoustic phonons; theoretically, these modes are Goldstone bosons of broken translation symmetry, and physically they correspond to the ions oscillating together in-phase in each of the three spatial directions. The dispersion of these modes is given by

$$\omega = c_s q, \tag{56}$$

where c_s is the speed of sound in the medium. Any remaining modes are gapped, meaning that at zero momentum transfer they have a non-zero excitation energy. All of these modes physically correspond to out-of-phase oscillations of the ions, which can set up an oscillating

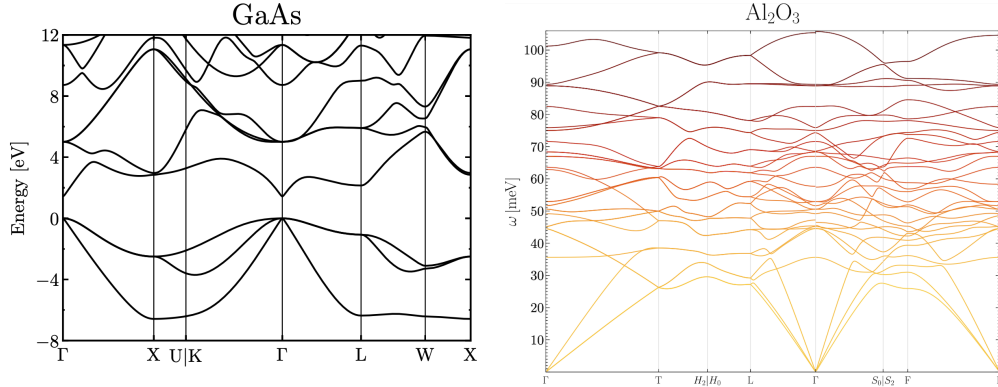


Figure 6. Band structure of two materials. (a) Electronic excitations in a semiconductor, GaAs. The Fermi energy defines the zero point on the y -axis, with the valence and conduction bands below and above the Fermi energy. On the x -axis, a slice is taken through the Brillouin zone to show a typical band structure. The Γ point is defined by where the bands come closest to crossing the Fermi surface. (b) Phonon excitations in a polar material, sapphire. Here the excitation energies (ω) are above the zero-energy state with no phonons. The Γ point is again defined by the point in momentum space where the gapless acoustic modes have zero energy, such that their dispersion is given by Equation 56. The gapped phonons are called optical, even though not all of these modes are optically active. Figure adapted from Reference [71].

dipole in the unit cell. The gapped phonons are called optical phonons because at least some of these modes are optically active. A typical band structure is shown in Figure 6.

Similar to the cases discussed above, the spin-independent scattering rate can be expressed in terms of a Dynamic Structure Factor,

$$S(\mathbf{q}, \omega) = \sum_{\nu} \frac{|F_{\nu}(\mathbf{q})|^2}{2\omega_{\nu, \mathbf{q}}} \delta(\omega_{\nu, \mathbf{q}} - \omega), \quad (57)$$

where $\omega_{\nu, \mathbf{q}}$ and $\epsilon_{\nu, \mathbf{q}, j}$ are the eigenvalues and eigenvectors of phonon branch ν (with the polarization vector indicating the direction in which ion j is oscillating, normalized such that $\sum_j |\epsilon_{\nu, \mathbf{q}, j}|^2 = 1$) of the coupled ionic oscillators, and $F_{\nu}(\mathbf{q})$ is a phonon form factor

$$|F_{\nu}(\mathbf{q})|^2 = \left| \sum_j \frac{e^{-W_j(\mathbf{q})}}{\sqrt{m_j}} \mathbf{q} \cdot \epsilon_{\nu, \mathbf{q}, j} e^{-i\mathbf{q} \cdot \mathbf{x}_j^0} \right|^2. \quad (58)$$

Here the sum runs over the ions at equilibrium position \mathbf{x}_j^0 in the unit cell, and W_j is the so-called Debye–Waller factor that acts as a form factor shutting off the phonon response

when the momentum transfer becomes larger than the inverse unit cell size $q \gtrsim a^{-1}$ (for a derivation and discussion, see References [52, 65, 89]). The eigenvalues and eigenvectors are typically obtained from a program like `PhonoPy` [90, 91] that computes the lattice force matrix on all n ions in the unit cell and diagonalizes it.

Operationally, the phonon form factor behaves similarly to the Helm form factor: It becomes highly suppressed when the effective description of collectively oscillating ions (or, in the case of the Helm, collective nucleons in a nucleus) breaks down due to resolving the internal structure of the unit cell. In particular, one can see explicitly that when the momentum transfer becomes large compared with the typical momentum in a mode, $q^2 \gg 2\omega_{\nu,q}m_j$, the Debye–Waller factor becomes large:

$$W_j(\mathbf{q}) = \frac{1}{4m_j} \sum_{\nu} \int_{\text{1BZ}} \frac{d^3k}{(2\pi)^3} \frac{|\mathbf{q} \cdot \epsilon_{\nu,\mathbf{k}j}|^2}{\omega_{\nu,\mathbf{k}}}, \quad (59)$$

and hence the Dynamic Structure Factor via the phonon form factor in Equation 58 becomes small. (Here the momentum has been integrated over the first Brillouin zone, denoted by 1BZ; for more detail, see Reference [65].) At a general momentum transfer, the phase factors, and in particular cancellations between the phase factors, can become important for accurately describing the DM interaction rate with phonons. However, at low momentum transfer, where the Debye–Waller factor is small, the form factor takes a simple form. For example, in a simple crystal like GaAs in which there are only two ions in the unit cell, we have

$$|F_{\nu}(\mathbf{q})|^2 \approx \frac{q^2}{2m_n} \left| \sqrt{A_{\text{Ga}}} e^{i\mathbf{x}_{\text{Ga}} \cdot \mathbf{q}} \pm \sqrt{A_{\text{As}}} e^{i\mathbf{x}_{\text{As}} \cdot \mathbf{q}} \right|^2, \quad (60)$$

where $\mathbf{x}_{\text{Ga,As}}$ and $A_{\text{Ga,As}}$ denote the positions and mass numbers of the gallium and arsenide ions in the unit cell, respectively [52]. In general, however, one uses codes employing DFT to compute the phonon eigenvectors and eigenfrequencies [65, 89]. This general program was outlined first in Reference [65], and a code implementing this program in a variety of materials is publicly available as the `PhonoDark` code [79, 92]. This code not only implements spin-independent interactions but also follows a general framework to calculate the DM single-phonon excitation rate via any Lorentz-invariant effective interaction. We describe this framework in the next section.

Experimental efforts are now underway to detect single collective excitations:

Collective mode	Target	Proposed materials	Gap?	Coupling
Acoustic phonon	All materials	He, Si, Ge, GaAs, Al ₂ O ₃ , diamond	No	$p/n/e^-$
Optical phonon	Polar, semiconductor	GaAs, Al ₂ O ₃	$\sim 10\text{--}100$ meV	$p/n/e^-$
Magnon	(Anti-)ferromagnet	Yttrium iron garnet	$\sim 0\text{--}10$ meV	e^-

Table II. Summary of the target materials that have been proposed for DM detection through collective excitations. The superconductor DM detection process is elastic for energy depositions well above the Cooper pair binding energy.

- The TESSERACT collaboration, consisting of the helium experiment HeRALD and the polar material experiment SPICE, is actively working to reach single optical phonon sensitivity with the transition edge sensors employed in the detector.
- To date, the single magnon proposal of References [73] and [93] has not been experimentally implemented, though a related concept (through many magnons) forms the basis of the QUAX experiment [94].

A summary of the collective modes, possible targets, gaps of each collective mode, and couplings (nucleon or electron) is given in Table II. We again refer the reader to Reference [88] for a currently complete discussion of ongoing experimental efforts.

An additional comment is in order: At typical energies above the higher optical mode (typically $\omega \sim 100$ meV) but below where the nucleus becomes definitely free ($\omega \sim 1$ eV), multiphonon emission becomes important. The calculation of multiphonon processes can rapidly become numerically intensive due to the large multiphonon phase space, and the presence of both harmonic and anharmonic multiphonon modes. Two-phonon production as a means to detect light DM was proposed in Reference [95] and [96] and was calculated in an EFT in References [97] and [98]. The harmonic contributions can be computed using analytic methods, the results can be applied to interpolate between the single phonon regime valid at low energies and the nuclear recoil regime [99], and the effect of anharmonicities can be estimated [100]. Note that even single phonon production will, initially, lead to the cascade of multiphonons [101] as the initial phonon decays through the anharmonic coupling, in a process rather analogous to showering.

C. In-Medium Effects

Small-gap electronic materials have a large in-medium response that affects the reach to DM scattering and absorption through screening effects. For isotropic, non-magnetic materials interacting through a dark photon, the effect of the in-medium response can be parameterized in terms of a reduced effective kinetic mixing parameter, ϵ_{eff} [24, 51]:

$$\epsilon_{\text{eff}} = \epsilon \frac{q^2}{q^2 - \Pi_{T,L}}, \quad (61)$$

where $\Pi_{T,L}$ is the in-medium polarization tensor of an isotropic, non-magnetic material related to the complex index of refraction \tilde{n} by $q^2(1 - \tilde{n}^2) = \Pi_L$ and $\omega^2(1 - \tilde{n}^2) = \Pi_T$. The case of an anisotropic material is significantly more involved [102]; the in-medium effects must be written in terms of a dielectric tensor, ϵ_{ij} , whose eigenvalues are given by

$$\pi_i = \omega^2(1 - \epsilon_{ii}), \quad (62)$$

with the effective mixing parameter

$$\epsilon_{\text{eff},i}^2 = \frac{\epsilon^2 m_{A'}^4}{[m_{A'}^2 - \text{Re}\pi_i(q)]^2 + [\text{Im}\pi_i(q)]^2}. \quad (63)$$

We discuss below how these effective couplings enter into the absorption rate.

VI. GENERALIZED DARK MATTER INTERACTIONS

We have summarized the relevant ingredients for DM to induce a response in a target material. We now generalize the framework to an EFT of DM scattering in Section VIA, followed by general considerations regarding DM absorption in target materials.

A. Effective Field Theory of Dark Matter Scattering with Collective Excitations

As suggested in Equation 45, one needs to be able to compute the transition matrix element $\langle f | \mathcal{F}_T(\mathbf{q}) | i \rangle$ for any interaction type in order to compute the DM scattering rate for any interaction type. This, in turn, implies that we must be able to compute the potential—the generalization of Equation 42—that the DM induces in the target material. DM is

a nonrelativistic state, and therefore one needs to follow the rules of non-relativistic EFT (NREFT). The discussion here largely follows Reference [79].

For scattering, the EFT calculation follows a simple plan:

1. Match relativistic operators onto non-relativistic operators. There is a long history in the nuclear physics literature of identifying the relevant nonrelativistic operators. They are

$$\mathbf{q} \equiv \mathbf{k}' - \mathbf{k}, \quad \mathbf{K} \equiv \mathbf{k}' + \mathbf{k}, \quad \mathbf{S}_\psi, \quad \mathbf{v}_\chi \equiv \frac{\mathbf{P}}{2m_\chi}, \quad \text{and} \quad \mathbf{v}_\psi \equiv \frac{\mathbf{K}}{2m_\psi}. \quad (64)$$

Here, m_ψ is the target fermion mass and \mathbf{S}_ψ is the spin. Note that in the nuclear recoil case, Galilean invariance is preserved, and the NREFT depends only on $\mathbf{v}^\perp \equiv \mathbf{v}_\chi - \mathbf{v}_\psi$. In the present case, in-medium effects may be important, and Galilean invariance is broken such that we need to keep both.

2. Equation 64 identifies charge, spin, and velocity operators as relevant to determining the potential created by the DM–target interaction. In particular, the transition matrix element induced by a potential, generalized from Equation 42 to include velocity and momentum dependence, is

$$\langle \nu, \mathbf{k} | \tilde{V}(\mathbf{q}, \mathbf{v}) | 0 \rangle = \sum_{\ell, j} \langle \nu, \mathbf{k} | e^{-i\mathbf{q} \cdot \mathbf{x}_{\ell j}} \tilde{V}_{\ell j}(\mathbf{q}, \mathbf{v}) | 0 \rangle, \quad (65)$$

where ℓ labels the unit cell, j denotes the ion within the unit cell, and the subscripts on the potential denote the contribution from each lattice site:

$$V(\mathbf{x}, \mathbf{v}) = \sum_{\ell j} V_{\ell j}(\mathbf{x} - \mathbf{x}_{\ell j}, \mathbf{v}), \quad (66)$$

with

$$\tilde{V}(\mathbf{q}, \mathbf{v}) = \int d^3x e^{-i\mathbf{q} \cdot \mathbf{x}} V(\mathbf{x}, \mathbf{v}). \quad (67)$$

The transition is between the ground state of the material $|0\rangle$ and a state with a single collective excitation, labeled $|\nu, \mathbf{k}\rangle$. Because in what follows we exclusively use the potential in momentum space, we hereafter drop the tilde on $\tilde{V}(\mathbf{q}, \mathbf{v})$ for readability.

3. Finally, we quantize the lattice potential to compute the matrix element. There are two quanta—phonons and magnons—that are excitations of the lattice potential that we consider.

- Phonons are quanta of lattice displacement $\mathbf{u}_{\ell j}$ from the equilibrium ion position at site j in the ℓ th unit cell $\mathbf{x}_{\ell j}^0$:

$$\mathbf{u}_{\ell j} = \mathbf{x}_{\ell j} - \mathbf{x}_{\ell j}^0 = \sum_{\nu=1}^{3n} \sum_{\mathbf{k}} \frac{1}{\sqrt{2Nm_j\omega_{\nu,\mathbf{k}}}} \left(\hat{a}_{\nu,\mathbf{k}} \epsilon_{\nu,\mathbf{k}j} e^{i\mathbf{k}\cdot\mathbf{x}_{\ell j}^0} + \hat{a}_{\nu,\mathbf{k}}^\dagger \epsilon_{\nu,\mathbf{k}j}^* e^{-i\mathbf{k}\cdot\mathbf{x}_{\ell j}^0} \right), \quad (68)$$

where N is the number of cells in the lattice, m_j is the mass of the ion at the j th site, and we have added subscripts on the energy deposition $\omega_{\nu,\mathbf{k}}$ (where the momentum \mathbf{k} is in the first Brillouin zone) to emphasize that the energy deposition must correspond to the energy of one of the eigenfrequencies of the collective excitations. Since the matrix element we seek to compute involves the potential from Equation 67 with a factor of $e^{i\mathbf{q}\cdot\mathbf{x}_{\ell j}}$, the matrix element must be evaluated via Campbell–Baker–Hausdorff to give¹

$$\langle \nu, \mathbf{k} | e^{-i\mathbf{q}\cdot\mathbf{x}_{\ell j}} V_{\ell j}(\mathbf{q}, \mathbf{v}) | 0 \rangle = \frac{1}{\sqrt{V}} \sum_{\nu,\mathbf{k}j} \left[\sum_{\ell} V_{\ell j}(\mathbf{q}, \mathbf{v}) e^{i(\mathbf{q}-\mathbf{k})\cdot\mathbf{x}_{\ell j}^0} \right] \frac{e^{-W_j(\mathbf{q})(\mathbf{q}\cdot\epsilon_{\nu,\mathbf{k}j}^*)}}{\sqrt{2m_j\omega_{\nu,\mathbf{k}}}}.$$

The task is then to evaluate the lattice potential, $V_{\ell j}(\mathbf{q}, \mathbf{v})$. This depends on the nature of the interaction. Using an example from Reference [79], involving four different types of responses, a lattice potential may take the following form:

$$V_{\ell j}(\mathbf{q}, \mathbf{v}) \supset \sum_{\alpha} \left[c_1 \langle e^{i\mathbf{q}\cdot\mathbf{x}_{\alpha}} \rangle_{\ell j} + c_4 \mathbf{S}_{\chi} \cdot \langle e^{i\mathbf{q}\cdot\mathbf{x}_{\alpha}} \mathbf{S}_{\alpha} \rangle_{\ell j} \right. \\ \left. + c_{8b} \mathbf{S}_{\chi} \cdot \langle e^{i\mathbf{q}\cdot\mathbf{x}_{\alpha}} \mathbf{v}_{\alpha} \rangle_{\ell j} + c_{3b} \frac{i\mathbf{q}}{m_{\psi}} \cdot \langle e^{i\mathbf{q}\cdot\mathbf{x}_{\alpha}} \mathbf{v}_{\alpha} \times \mathbf{S}_{\alpha} \rangle_{\ell j} \right]. \quad (69)$$

A spin-independent interaction requires one to evaluate the matrix element

$$\sum_{\alpha} \langle e^{i\mathbf{q}\cdot\mathbf{x}_{\alpha}} \rangle_{\ell j} \simeq \langle N_{\psi} \rangle_{\ell j}, \quad (70)$$

where α runs over fermions of type $\psi = p, n, e$. Likewise, a spin-dependent interaction requires one to evaluate

$$\sum_{\alpha} \langle e^{i\mathbf{q}\cdot\mathbf{x}_{\alpha}} \mathbf{S}_{\psi,\alpha} \rangle_{\ell j} \simeq \langle \mathbf{S}_{\psi} \rangle_{\ell j}. \quad (71)$$

Coupling to electric and magnetic dipoles, as well as the anapole operator, involves the velocity $\mathbf{v}_{\psi,\alpha} = -\frac{i}{2m_{\psi}} \overleftrightarrow{\nabla}$, and one must evaluate the expectation value,

$$\sum_{\alpha} \langle e^{i\mathbf{q}\cdot\mathbf{x}_{\alpha}} \mathbf{v}_{\psi,\alpha} \rangle_{\ell j} \simeq i \langle (\mathbf{q} \cdot \mathbf{x}_{\alpha}) \mathbf{v}_{\psi,\alpha} \rangle_{\ell j}, \quad (72)$$

¹ the derivation can be found in Reference [65].

which becomes

$$\langle x_\alpha^i v_{\psi,\alpha}^k \rangle_{\ell j} = -\frac{i}{2m_\psi} \langle x^i \nabla_\alpha^k - x^k \nabla_\alpha^i \rangle_{\ell j} = \frac{1}{2m_\psi} \epsilon_{ikk'} \langle L_\alpha^{k'} \rangle_{\ell j}, \quad (73)$$

where L is an angular momentum operator. Overall, one finds in the long-wavelength limit that there are four types of responses:

$$N, \quad S, \quad L, \quad \text{and} \quad L \otimes S, \quad (74)$$

where we have not written out the decomposition of the last operator because it does not commonly appear in Lorentz-invariant ultraviolet-completions.

- Magnons are quanta of spin precession. Here, the relevant matrix element is

$$\langle \nu, \mathbf{k} | V(\mathbf{q}, \mathbf{v}) | 0 \rangle = \sum_{\ell, j} e^{i\mathbf{q} \cdot \mathbf{x}_{\ell j}} \mathbf{f}_j(\mathbf{q}, \mathbf{v}) \cdot \langle \nu, \mathbf{k} | \mathbf{S}_{\ell j} | 0 \rangle, \quad (75)$$

where \mathbf{f}_j is dependent on the interaction type, and $\mathbf{S}_{\ell j}$ denotes the ion effective spins, which can come both from electronic spin and orbital angular momentum (for details, see References [79] and [73]). This shows that one needs a net spin on each unit cell to excite a response.

The rate is then computed from Fermi's Golden Rule (Equation 39), which in the case at hand becomes

$$\Gamma(\mathbf{v}) = \int \frac{d^3 q}{(2\pi)^3} \sum_{\nu, \mathbf{k}} \left| \sum_{\ell, j} \langle \nu, \mathbf{k} | e^{-i\mathbf{q} \cdot \mathbf{x}_{\ell j}} V_{\ell j}(\mathbf{q}, \mathbf{v}) | 0 \rangle \right|^2 2\pi \delta(E_f - E_i - \omega). \quad (76)$$

B. Target Response to Dark Matter Absorption

In this subsection, we discuss DM absorption in materials, and focus on the case of vector DM and pseudoscalar (axion) DM. For the case of absorption, the energy absorbed is simply the mass, $\omega = m_\chi$, which is much greater than the momentum, $q = m_\chi v$, $\omega \gg q$. This implies one of two possibilities to kinematically allow for DM absorption:

1. an inelastic transition in the target material, implying the presence of a gapped mode having $\omega_q \neq 0$ as $q \rightarrow 0$; or

2. an absorption process with two excitations in the final state, where the momenta of the two excitations cancel (to high precision) while the sum of their energies equals m_χ .

It has long been appreciated that new particles (produced in the Sun) can be absorbed on target materials via inelastic transitions [103, 104], such as valence electrons in semiconductors making a valence-to-conduction-band transition. More recently, these ideas were applied to vector axion DM absorption on electrons in xenon [105, 106]. The absorption rate can be related to the complex conductivity via the optical theorem

$$\Gamma_\gamma = -\frac{\text{Im}\Pi(\omega)}{\omega}, \quad (77)$$

where Π is related to the complex conductivity $\hat{\sigma}(\omega)$:

$$\Pi(\omega) \approx -i\hat{\sigma}\omega, \quad (78)$$

with Π having transverse and longitudinal polarizations as in Equation 61. Since $|\mathbf{q}| \ll \omega$, $\Pi_L = \Pi_T \simeq \Pi$. The dark photon absorption rate, per unit of target mass, is given by

$$\Gamma_{A'} = \frac{1}{\rho_T} \frac{\rho_\chi}{m_\chi} \epsilon_{\text{eff}}^2 \Gamma_\gamma, \quad (79)$$

with ϵ_{eff} (for an isotropic non-magnetic medium) given by Equation 61. For an anisotropic material, the absorption rate, per unit of target mass, is as follows [102]:

$$R = -\frac{1}{3} \frac{\rho_\chi}{\rho_T} \sum_{i=1}^3 \epsilon_{\text{eff},i}^2 \frac{\text{Im}\pi_i(q)}{m_{A'}^2}, \quad (80)$$

where π_i denotes the eigenvalues of the polarization tensor.

The axion absorption rate on electrons can be extracted from Equation 77 by using the relation with the photon absorption rate [107]:

$$|\mathcal{M}|^2 \approx 3(g_{aee}/2m_e)^2 (m_a/e)^2 |\mathcal{M}_\gamma|^2. \quad (81)$$

Axions can also be absorbed on gapped optical phonons [93]. These modes, similar to electrons in a semiconductor, have a gap at zero momentum transfer (see Figure 6). Unlike the case of absorption on electrons, where one can make use of the direct axion electron coupling, the interaction goes via the mixing of the phonon with the photon (known as the phonon polariton), in the presence of an external B field.

In the second process enumerated above, two modes recoil against each other. In this case, the momentum can be conserved by a cancellation between the two outgoing modes; this cancellation is necessary for acoustic phonons because, for a fixed energy deposition, they have a large amount of momentum compared with the DM momentum due to the small speed of sound compared with the DM velocity, $c_s \ll v_\chi$:

$$q_{\text{ph}} = \frac{\omega}{c_s} \gg \frac{\omega}{v_\chi}. \quad (82)$$

For example, bosonic DM can be absorbed on free electrons in superconductors by emitting a phonon [108], on two gapless phonons in superfluid helium [96], or on a photon and phonon [109]. All become kinematically possible because of the back-to-back recoil of the two final-state excitations. Note that in the cases where only one excitation is produced (*e.g.* electron or optical phonon excitation in semiconductors), momentum is conserved by recoil against the lattice.

A summary plot comparing the reach of axion and dark photon absorption on electrons in semiconductors and superconductors, and on phonon polaritons in polar crystals, is shown in Figure 7.

Here, we have chosen to restrict ourselves to particular models whose absorption rate can be simply related to photon interaction rates. One can also pursue an EFT framework for absorption on both electrons [76, 110] and collective modes (phonons [92] and magnons [73]). We direct the reader to the references cited here for further details on more general types of interactions, including DM absorption via electric and magnetic dipoles.

VII. CONCLUSION

We have reviewed the development of theories of particle DM of a very low mass—below the traditional WIMP window of ~ 10 GeV but above masses of ~ 1 eV, where DM becomes wavelike (*e.g.* axions). Such models are motivated by hidden-sector theories and have rich cosmological and astrophysical dynamics, from self-interactions to impacts on stellar evolution and observational consequences in collider experiments. We have reviewed the astrophysical, cosmological and collider constraints most directly relevant for the model space in terrestrial direct detection experiments.

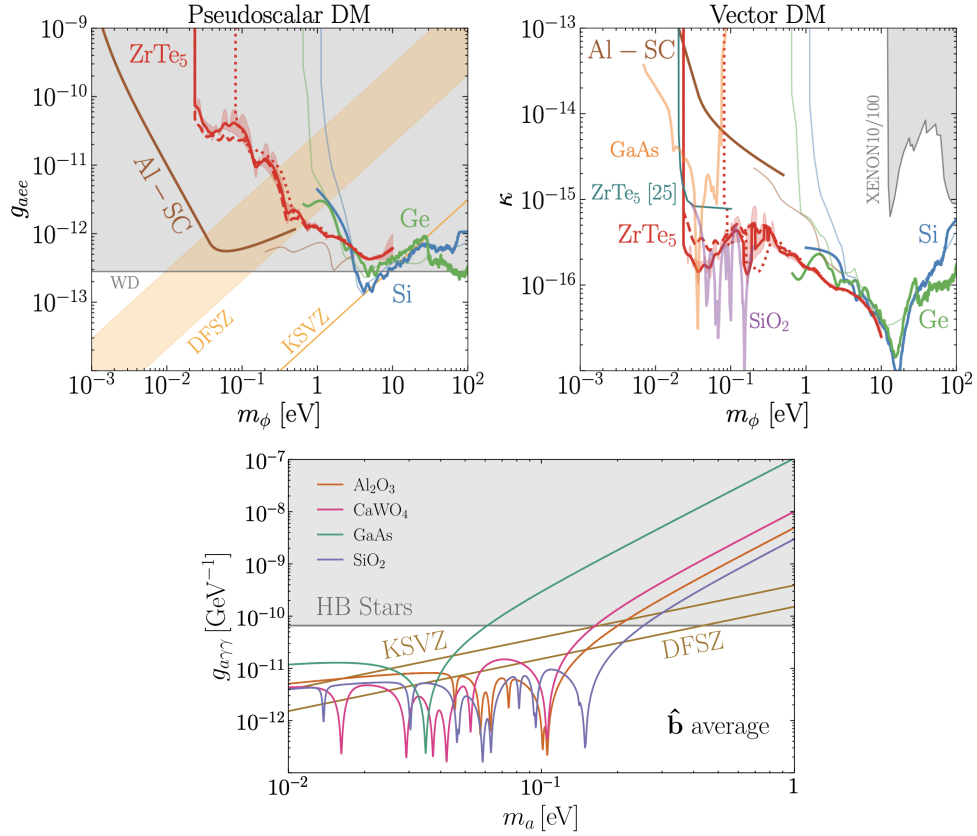


Figure 7. *Upper*: Reach to (a) axion DM and (b) vector DM via their (a) electron coupling or (b) kinetic mixing coupling to the target material, for 1-kg-year exposure. (c) Reach to axion DM by absorption on phonon polaritons in a 1-T external magnetic field. Abbreviations: Al SC, superconducting aluminum; DM, dark matter; HB, horizontal branch; WD, white dwarf. Panels *a* and *b* adapted from Reference [76]. Panel *c* adapted from Reference [93].

While 15 years ago, direct detection experiments could not reach the sub-GeV DM mass window, the proposal of HVDM/HSDM led to an explosion of ideas for direct detection experiments. A subsequent push in the last 5-10 years to realize these experiments with research and development gave rise to funded experiments that are actively reaching new theory space. At the present moment, these experimental efforts have not yet covered the best-motivated candidates, such as asymmetric DM, thermal freeze-out DM, and DM produced through freeze-in. As these new experiments come to fruition and push to lower cross sections with better handles on backgrounds and systematic uncertainties, we look forward

to the possible uncovering of the Universe’s dark side.

DISCLOSURE STATEMENT

The author is not aware of any affiliations, memberships, funding, or financial holdings that might be perceived as affecting the objectivity of this review.

ACKNOWLEDGMENTS

I thank Yufeng Du, Osmond Wen, Zhengkang Zhang, and especially Clara Murgui and Tanner Trickle for a careful reading of the manuscript. This work was supported by the US Department of Energy, Office of Science, Quantum Information Science Enabled Discovery (QuantISED) for High Energy Physics (KA2401032), by the Office of High Energy Physics (award DE-SC0011632), by a Simons Investigator Award, and by the Walter Burke Institute for Theoretical Physics.

-
- [1] G. Bertone, D. Hooper, and J. Silk, Particle dark matter: Evidence, candidates and constraints, *Phys. Rept.* **405**, 279 (2005), arXiv:hep-ph/0404175.
 - [2] J. Cooley *et al.*, Report of the Topical Group on Particle Dark Matter for Snowmass 2021, (2022), arXiv:2209.07426 [hep-ph].
 - [3] C. B. Adams *et al.*, Axion Dark Matter, *Snowmass 2021*, (2022), arXiv:2203.14923 [hep-ex].
 - [4] N. Afshordi, P. McDonald, and D. N. Spergel, Primordial black holes as dark matter: The Power spectrum and evaporation of early structures, *Astrophys. J. Lett.* **594**, L71 (2003), arXiv:astro-ph/0302035.
 - [5] H. Ramani, T. Trickle, and K. M. Zurek, Observability of Dark Matter Substructure with Pulsar Timing Correlations, *JCAP* **12**, 033, arXiv:2005.03030 [astro-ph.CO].
 - [6] K. Van Tilburg, A.-M. Taki, and N. Weiner, Halometry from Astrometry, *JCAP* **07**, 041, arXiv:1804.01991 [astro-ph.CO].
 - [7] M. I. Gresham, V. S. H. Lee, and K. M. Zurek, Astrophysical observations of a dark matter-Baryon fifth force, *JCAP* **02**, 048, arXiv:2209.03963 [astro-ph.HE].

- [8] M. Battaglieri *et al.*, US Cosmic Visions: New Ideas in Dark Matter 2017: Community Report, in *U.S. Cosmic Visions: New Ideas in Dark Matter* (2017) arXiv:1707.04591 [hep-ph].
- [9] E. O. Nadler *et al.* (DES), Milky Way Satellite Census. III. Constraints on Dark Matter Properties from Observations of Milky Way Satellite Galaxies, *Phys. Rev. Lett.* **126**, 091101 (2021), arXiv:2008.00022 [astro-ph.CO].
- [10] M. J. Strassler and K. M. Zurek, Echoes of a hidden valley at hadron colliders, *Phys. Lett. B* **651**, 374 (2007), arXiv:hep-ph/0604261.
- [11] M. J. Strassler and K. M. Zurek, Discovering the Higgs through highly-displaced vertices, *Phys. Lett. B* **661**, 263 (2008), arXiv:hep-ph/0605193.
- [12] C. Boehm and P. Fayet, Scalar dark matter candidates, *Nucl. Phys. B* **683**, 219 (2004), arXiv:hep-ph/0305261.
- [13] M. Pospelov, A. Ritz, and M. B. Voloshin, Secluded WIMP Dark Matter, *Phys. Lett. B* **662**, 53 (2008), arXiv:0711.4866 [hep-ph].
- [14] M. Pospelov and A. Ritz, Astrophysical Signatures of Secluded Dark Matter, *Phys. Lett. B* **671**, 391 (2009), arXiv:0810.1502 [hep-ph].
- [15] D. E. Kaplan, M. A. Luty, and K. M. Zurek, Asymmetric Dark Matter, *Phys. Rev. D* **79**, 115016 (2009), arXiv:0901.4117 [hep-ph].
- [16] K. M. Zurek, Asymmetric Dark Matter: Theories, Signatures, and Constraints, *Phys. Rept.* **537**, 91 (2014), arXiv:1308.0338 [hep-ph].
- [17] D. E. Kaplan, G. Z. Krnjaic, K. R. Rehermann, and C. M. Wells, Atomic Dark Matter, *JCAP* **05**, 021, arXiv:0909.0753 [hep-ph].
- [18] G. D. Kribs, T. S. Roy, J. Terning, and K. M. Zurek, Quirky Composite Dark Matter, *Phys. Rev. D* **81**, 095001 (2010), arXiv:0909.2034 [hep-ph].
- [19] K. K. Boddy, J. L. Feng, M. Kaplinghat, and T. M. P. Tait, Self-Interacting Dark Matter from a Non-Abelian Hidden Sector, *Phys. Rev. D* **89**, 115017 (2014), arXiv:1402.3629 [hep-ph].
- [20] J. L. Feng and J. Kumar, The WIMPlless Miracle: Dark-Matter Particles without Weak-Scale Masses or Weak Interactions, *Phys. Rev. Lett.* **101**, 231301 (2008), arXiv:0803.4196 [hep-ph].
- [21] Y. Hochberg, E. Kuflik, H. Murayama, T. Volansky, and J. G. Wacker, Model for Thermal Relic Dark Matter of Strongly Interacting Massive Particles, *Phys. Rev. Lett.* **115**, 021301

- (2015), arXiv:1411.3727 [hep-ph].
- [22] B. Holdom, Two U(1)'s and Epsilon Charge Shifts, Phys. Lett. B **166**, 196 (1986).
 - [23] D. Hooper and K. M. Zurek, A Natural Supersymmetric Model with MeV Dark Matter, Phys. Rev. D **77**, 087302 (2008), arXiv:0801.3686 [hep-ph].
 - [24] S. Knapen, T. Lin, and K. M. Zurek, Light Dark Matter: Models and Constraints, Phys. Rev. D **96**, 115021 (2017), arXiv:1709.07882 [hep-ph].
 - [25] B. Patt and F. Wilczek, Higgs-field portal into hidden sectors, (2006), arXiv:hep-ph/0605188.
 - [26] D. Hooper, J. March-Russell, and S. M. West, Asymmetric sneutrino dark matter and the Omega(b) / Omega(DM) puzzle, Phys. Lett. B **605**, 228 (2005), arXiv:hep-ph/0410114.
 - [27] S. Alekhin *et al.*, A facility to Search for Hidden Particles at the CERN SPS: the SHiP physics case, Rept. Prog. Phys. **79**, 124201 (2016), arXiv:1504.04855 [hep-ph].
 - [28] C. Murgui and K. M. Zurek, Dark unification: A UV-complete theory of asymmetric dark matter, Phys. Rev. D **105**, 095002 (2022), arXiv:2112.08374 [hep-ph].
 - [29] T. Cohen, D. J. Phalen, A. Pierce, and K. M. Zurek, Asymmetric Dark Matter from a GeV Hidden Sector, Phys. Rev. D **82**, 056001 (2010), arXiv:1005.1655 [hep-ph].
 - [30] S. Galli, F. Iocco, G. Bertone, and A. Melchiorri, Updated CMB constraints on Dark Matter annihilation cross-sections, Phys. Rev. D **84**, 027302 (2011), arXiv:1106.1528 [astro-ph.CO].
 - [31] D. P. Finkbeiner, S. Galli, T. Lin, and T. R. Slatyer, Searching for Dark Matter in the CMB: A Compact Parameterization of Energy Injection from New Physics, Phys. Rev. D **85**, 043522 (2012), arXiv:1109.6322 [astro-ph.CO].
 - [32] T. Lin, H.-B. Yu, and K. M. Zurek, On Symmetric and Asymmetric Light Dark Matter, Phys. Rev. D **85**, 063503 (2012), arXiv:1111.0293 [hep-ph].
 - [33] M. S. Madhavacheril, N. Sehgal, and T. R. Slatyer, Current Dark Matter Annihilation Constraints from CMB and Low-Redshift Data, Phys. Rev. D **89**, 103508 (2014), arXiv:1310.3815 [astro-ph.CO].
 - [34] C. Boehm, P. Fayet, and J. Silk, Light and heavy dark matter particles, Phys. Rev. D **69**, 101302 (2004), arXiv:hep-ph/0311143.
 - [35] D. Hooper, M. Kaplinghat, L. E. Strigari, and K. M. Zurek, MeV Dark Matter and Small Scale Structure, Phys. Rev. D **76**, 103515 (2007), arXiv:0704.2558 [astro-ph].

- [36] M. L. Graesser, I. M. Shoemaker, and L. Vecchi, Asymmetric WIMP dark matter, *JHEP* **10**, 110, arXiv:1103.2771 [hep-ph].
- [37] L. J. Hall, K. Jedamzik, J. March-Russell, and S. M. West, Freeze-In Production of FIMP Dark Matter, *JHEP* **03**, 080, arXiv:0911.1120 [hep-ph].
- [38] C. Dvorkin, T. Lin, and K. Schutz, Making dark matter out of light: freeze-in from plasma effects, *Phys. Rev. D* **99**, 115009 (2019), [Erratum: *Phys.Rev.D* 105, 119901 (2022)], arXiv:1902.08623 [hep-ph].
- [39] X. Chu, T. Hambye, and M. H. G. Tytgat, The Four Basic Ways of Creating Dark Matter Through a Portal, *JCAP* **05**, 034, arXiv:1112.0493 [hep-ph].
- [40] Y. Hochberg, E. Kuflik, T. Volansky, and J. G. Wacker, Mechanism for Thermal Relic Dark Matter of Strongly Interacting Massive Particles, *Phys. Rev. Lett.* **113**, 171301 (2014), arXiv:1402.5143 [hep-ph].
- [41] E. Kuflik, M. Perelstein, N. R.-L. Lorier, and Y.-D. Tsai, Phenomenology of ELDER Dark Matter, *JHEP* **08**, 078, arXiv:1706.05381 [hep-ph].
- [42] E. D. Carlson, M. E. Machacek, and L. J. Hall, Self-interacting dark matter, *Astrophys. J.* **398**, 43 (1992).
- [43] A. A. de Laix, R. J. Scherrer, and R. K. Schaefer, Constraints of selfinteracting dark matter, *Astrophys. J.* **452**, 495 (1995), arXiv:astro-ph/9502087.
- [44] E. Kuflik, M. Perelstein, N. R.-L. Lorier, and Y.-D. Tsai, Elastically Decoupling Dark Matter, *Phys. Rev. Lett.* **116**, 221302 (2016), arXiv:1512.04545 [hep-ph].
- [45] T.-H. Yeh, K. A. Olive, and B. D. Fields, The impact of new $d(p, \gamma)3$ rates on Big Bang Nucleosynthesis, *JCAP* **03**, 046, arXiv:2011.13874 [astro-ph.CO].
- [46] T.-H. Yeh, J. Shelton, K. A. Olive, and B. D. Fields, Probing physics beyond the standard model: limits from BBN and the CMB independently and combined, *JCAP* **10**, 046, arXiv:2207.13133 [astro-ph.CO].
- [47] W. Enzi *et al.*, Joint constraints on thermal relic dark matter from strong gravitational lensing, the Ly α forest, and Milky Way satellites, *Mon. Not. Roy. Astron. Soc.* **506**, 5848 (2021), arXiv:2010.13802 [astro-ph.CO].
- [48] A. E. Nelson and J. Scholtz, Dark Light, Dark Matter and the Misalignment Mechanism, *Phys. Rev. D* **84**, 103501 (2011), arXiv:1105.2812 [hep-ph].

- [49] P. W. Graham, J. Mardon, and S. Rajendran, Vector Dark Matter from Inflationary Fluctuations, *Phys. Rev. D* **93**, 103520 (2016), arXiv:1504.02102 [hep-ph].
- [50] S. Tulin and H.-B. Yu, Dark Matter Self-interactions and Small Scale Structure, *Phys. Rept.* **730**, 1 (2018), arXiv:1705.02358 [hep-ph].
- [51] Y. Hochberg, M. Pyle, Y. Zhao, and K. M. Zurek, Detecting Superlight Dark Matter with Fermi-Degenerate Materials, *JHEP* **08**, 057, arXiv:1512.04533 [hep-ph].
- [52] S. Knapen, T. Lin, M. Pyle, and K. M. Zurek, Detection of Light Dark Matter With Optical Phonons in Polar Materials, *Phys. Lett. B* **785**, 386 (2018), arXiv:1712.06598 [hep-ph].
- [53] G. G. Raffelt, *Stars as laboratories for fundamental physics: The astrophysics of neutrinos, axions, and other weakly interacting particles* (1996).
- [54] J. H. Chang, R. Essig, and S. D. McDermott, Supernova 1987A Constraints on Sub-GeV Dark Sectors, Millicharged Particles, the QCD Axion, and an Axion-like Particle, *JHEP* **09**, 051, arXiv:1803.00993 [hep-ph].
- [55] M. Baryakhtar, J. Bramante, S. W. Li, T. Linden, and N. Raj, Dark Kinetic Heating of Neutron Stars and An Infrared Window On WIMPs, SIMPs, and Pure Higgsinos, *Phys. Rev. Lett.* **119**, 131801 (2017), arXiv:1704.01577 [hep-ph].
- [56] M. Taoso, F. Iocco, G. Meynet, G. Bertone, and P. Eggenberger, Effect of low mass dark matter particles on the Sun, *Phys. Rev. D* **82**, 083509 (2010), arXiv:1005.5711 [astro-ph.CO].
- [57] A. R. Zentner and A. P. Hearin, Asymmetric Dark Matter May Alter the Evolution of Low-mass Stars and Brown Dwarfs, *Phys. Rev. D* **84**, 101302 (2011), arXiv:1110.5919 [astro-ph.CO].
- [58] S. C. Leung, M. C. Chu, L. M. Lin, and K. W. Wong, Dark-matter admixed white dwarfs, *Phys. Rev. D* **87**, 123506 (2013), arXiv:1305.6142 [astro-ph.CO].
- [59] P. W. Graham, R. Janish, V. Narayan, S. Rajendran, and P. Riggins, White Dwarfs as Dark Matter Detectors, *Phys. Rev. D* **98**, 115027 (2018), arXiv:1805.07381 [hep-ph].
- [60] A. Joglekar, N. Raj, P. Tanedo, and H.-B. Yu, Dark kinetic heating of neutron stars from contact interactions with relativistic targets, *Phys. Rev. D* **102**, 123002 (2020), arXiv:2004.09539 [hep-ph].
- [61] E. Izaguirre, G. Krnjaic, P. Schuster, and N. Toro, New Electron Beam-Dump Experiments to Search for MeV to few-GeV Dark Matter, *Phys. Rev. D* **88**, 114015 (2013), arXiv:1307.6554

- [hep-ph].
- [62] E. Izaguirre, G. Krnjaic, P. Schuster, and N. Toro, Testing GeV-Scale Dark Matter with Fixed-Target Missing Momentum Experiments, *Phys. Rev. D* **91**, 094026 (2015), arXiv:1411.1404 [hep-ph].
- [63] J. D. Bjorken, R. Essig, P. Schuster, and N. Toro, New Fixed-Target Experiments to Search for Dark Gauge Forces, *Phys. Rev. D* **80**, 075018 (2009), arXiv:0906.0580 [hep-ph].
- [64] S. Andreas, C. Niebuhr, and A. Ringwald, New Limits on Hidden Photons from Past Electron Beam Dumps, *Phys. Rev. D* **86**, 095019 (2012), arXiv:1209.6083 [hep-ph].
- [65] T. Trickle, Z. Zhang, K. M. Zurek, K. Inzani, and S. M. Griffin, Multi-Channel Direct Detection of Light Dark Matter: Theoretical Framework, *JHEP* **03**, 036, arXiv:1910.08092 [hep-ph].
- [66] R. Essig, J. Mardon, and T. Volansky, Direct Detection of Sub-GeV Dark Matter, *Phys. Rev. D* **85**, 076007 (2012), arXiv:1108.5383 [hep-ph].
- [67] P. W. Graham, D. E. Kaplan, S. Rajendran, and M. T. Walters, Semiconductor Probes of Light Dark Matter, *Phys. Dark Univ.* **1**, 32 (2012), arXiv:1203.2531 [hep-ph].
- [68] R. Essig, M. Fernandez-Serra, J. Mardon, A. Soto, T. Volansky, and T.-T. Yu, Direct Detection of sub-GeV Dark Matter with Semiconductor Targets, *JHEP* **05**, 046, arXiv:1509.01598 [hep-ph].
- [69] Y. Hochberg, Y. Kahn, M. Lisanti, K. M. Zurek, A. G. Grushin, R. Ilan, S. M. Griffin, Z.-F. Liu, S. F. Weber, and J. B. Neaton, Detection of sub-MeV Dark Matter with Three-Dimensional Dirac Materials, *Phys. Rev. D* **97**, 015004 (2018), arXiv:1708.08929 [hep-ph].
- [70] R. Essig, J. Mardon, O. Slone, and T. Volansky, Detection of sub-GeV Dark Matter and Solar Neutrinos via Chemical-Bond Breaking, *Phys. Rev. D* **95**, 056011 (2017), arXiv:1608.02940 [hep-ph].
- [71] S. M. Griffin, K. Inzani, T. Trickle, Z. Zhang, and K. M. Zurek, Multichannel direct detection of light dark matter: Target comparison, *Phys. Rev. D* **101**, 055004 (2020), arXiv:1910.10716 [hep-ph].
- [72] R. Anthony-Petersen *et al.*, A Stress Induced Source of Phonon Bursts and Quasiparticle Poisoning, (2022), arXiv:2208.02790 [physics.ins-det].

- [73] T. Trickle, Z. Zhang, and K. M. Zurek, Detecting Light Dark Matter with Magnons, *Phys. Rev. Lett.* **124**, 201801 (2020), arXiv:1905.13744 [hep-ph].
- [74] C. Blanco, J. I. Collar, Y. Kahn, and B. Lillard, Dark Matter-Electron Scattering from Aromatic Organic Targets, *Phys. Rev. D* **101**, 056001 (2020), arXiv:1912.02822 [hep-ph].
- [75] Y. Hochberg, Y. Zhao, and K. M. Zurek, Superconducting Detectors for Superlight Dark Matter, *Phys. Rev. Lett.* **116**, 011301 (2016), arXiv:1504.07237 [hep-ph].
- [76] H.-Y. Chen, A. Mitridate, T. Trickle, Z. Zhang, M. Bernardi, and K. M. Zurek, Dark matter direct detection in materials with spin-orbit coupling, *Phys. Rev. D* **106**, 015024 (2022), arXiv:2202.11716 [hep-ph].
- [77] Y. Hochberg, Y. Kahn, N. Kurinsky, B. V. Lehmann, T. C. Yu, and K. K. Berggren, Determining Dark-Matter–Electron Scattering Rates from the Dielectric Function, *Phys. Rev. Lett.* **127**, 151802 (2021), arXiv:2101.08263 [hep-ph].
- [78] P. Du, D. Egaña Ugrinovic, R. Essig, and M. Sholapurkar, Doped Semiconductor Devices for sub-MeV Dark Matter Detection, (2022), arXiv:2212.04504 [hep-ph].
- [79] T. Trickle, Z. Zhang, and K. M. Zurek, Effective field theory of dark matter direct detection with collective excitations, *Phys. Rev. D* **105**, 015001 (2022), arXiv:2009.13534 [hep-ph].
- [80] S. M. Griffin, K. Inzani, T. Trickle, Z. Zhang, and K. M. Zurek, Extended calculation of dark matter-electron scattering in crystal targets, *Phys. Rev. D* **104**, 095015 (2021), arXiv:2105.05253 [hep-ph].
- [81] S. K. Lee, M. Lisanti, S. Mishra-Sharma, and B. R. Safdi, Modulation Effects in Dark Matter–Electron Scattering Experiments, *Phys. Rev. D* **92**, 083517 (2015), arXiv:1508.07361 [hep-ph].
- [82] Y. Hochberg, Y. Kahn, M. Lisanti, C. G. Tully, and K. M. Zurek, Directional detection of dark matter with two-dimensional targets, *Phys. Lett. B* **772**, 239 (2017), arXiv:1606.08849 [hep-ph].
- [83] C. E. Dreyer, R. Essig, M. Fernandez-Serra, A. Singal, and C. Zhen, Fully ab-initio all-electron calculation of dark matter–electron scattering in crystals with evaluation of systematic uncertainties, (2023), arXiv:2306.14944 [hep-ph].
- [84] T. Trickle, Extended calculation of electronic excitations for direct detection of dark matter, *Phys. Rev. D* **107**, 035035 (2023), arXiv:2210.14917 [hep-ph].

- [85] S. Knapen, J. Kozaczuk, and T. Lin, python package for dark matter scattering in dielectric targets, *Phys. Rev. D* **105**, 015014 (2022), arXiv:2104.12786 [hep-ph].
- [86] S. Knapen, J. Kozaczuk, and T. Lin, Dark matter-electron scattering in dielectrics, *Phys. Rev. D* **104**, 015031 (2021), arXiv:2101.08275 [hep-ph].
- [87] Y. Hochberg, B. V. Lehmann, I. Charaev, J. Chiles, M. Colangelo, S. W. Nam, and K. K. Berggren, New constraints on dark matter from superconducting nanowires, *Phys. Rev. D* **106**, 112005 (2022), arXiv:2110.01586 [hep-ph].
- [88] R. Essig *et al.*, Snowmass2021 Cosmic Frontier: The landscape of low-threshold dark matter direct detection in the next decade, in *Snowmass 2021* (2022) arXiv:2203.08297 [hep-ph].
- [89] S. Griffin, S. Knapen, T. Lin, and K. M. Zurek, Directional Detection of Light Dark Matter with Polar Materials, *Phys. Rev. D* **98**, 115034 (2018), arXiv:1807.10291 [hep-ph].
- [90] A. Togo, L. Chaput, T. Tadano, and I. Tanaka, Implementation strategies in phonopy and phono3py, *J. Phys. Condens. Matter* **35**, 353001 (2023).
- [91] A. Togo, First-principles phonon calculations with phonopy and phono3py, *J. Phys. Soc. Jpn.* **92**, 012001 (2023).
- [92] A. Mitridate, K. Pardo, T. Trickle, and K. M. Zurek, Effective Field Theory for Dark Matter Absorption on Single Phonons, (2023), arXiv:2308.06314 [hep-ph].
- [93] A. Mitridate, T. Trickle, Z. Zhang, and K. M. Zurek, Detectability of Axion Dark Matter with Phonon Polaritons and Magnons, *Phys. Rev. D* **102**, 095005 (2020), arXiv:2005.10256 [hep-ph].
- [94] N. Crescini *et al.* (QUAX), Axion search with a quantum-limited ferromagnetic haloscope, *Phys. Rev. Lett.* **124**, 171801 (2020), arXiv:2001.08940 [hep-ex].
- [95] K. Schutz and K. M. Zurek, Detectability of Light Dark Matter with Superfluid Helium, *Phys. Rev. Lett.* **117**, 121302 (2016), arXiv:1604.08206 [hep-ph].
- [96] S. Knapen, T. Lin, and K. M. Zurek, Light Dark Matter in Superfluid Helium: Detection with Multi-excitation Production, *Phys. Rev. D* **95**, 056019 (2017), arXiv:1611.06228 [hep-ph].
- [97] A. Caputo, A. Esposito, and A. D. Polosa, Light Dark Matter and Superfluid He-4 from EFT, *J. Phys. Conf. Ser.* **1468**, 012060 (2020), arXiv:1911.07867 [hep-ph].
- [98] F. Acanfora, A. Esposito, and A. D. Polosa, Sub-GeV Dark Matter in Superfluid He-4: an Effective Theory Approach, *Eur. Phys. J. C* **79**, 549 (2019), arXiv:1902.02361 [hep-ph].

- [99] B. Campbell-Deem, S. Knapen, T. Lin, and E. Villarama, Dark matter direct detection from the single phonon to the nuclear recoil regime, *Phys. Rev. D* **106**, 036019 (2022), arXiv:2205.02250 [hep-ph].
- [100] T. Lin, C.-H. Shen, M. Sholapurkar, and E. Villarama, Anharmonic effects in nuclear recoils from sub-GeV dark matter, (2023), arXiv:2309.10839 [hep-ph].
- [101] G. Baym, D. H. Beck, J. P. Filippini, C. J. Pethick, and J. Shelton, Searching for low mass dark matter via phonon creation in superfluid ^4He , *Phys. Rev. D* **102**, 035014 (2020), [Erratum: *Phys.Rev.D* 104, 019901 (2021)], arXiv:2005.08824 [hep-ph].
- [102] A. Coskuner, A. Mitridate, A. Olivares, and K. M. Zurek, Directional Dark Matter Detection in Anisotropic Dirac Materials, *Phys. Rev. D* **103**, 016006 (2021), arXiv:1909.09170 [hep-ph].
- [103] S. Dimopoulos, G. D. Starkman, and B. W. Lynn, Atomic Enhancements in the Detection of Axions, *Mod. Phys. Lett. A* **1**, 491 (1986).
- [104] G. Gelmini, S. P. Ahlen, F. T. Avignone, R. L. Brodzinski, S. Dimopoulos, A. K. Drukier, B. W. Lynn, D. N. Spergel, and G. D. Starkman, BOUNDS FROM DIRECT SEARCH OF GALACTIC COLD DARK MATTER AND SOLAR AXIONS FROM A GE SPECTROMETER (1987).
- [105] M. Pospelov, A. Ritz, and M. B. Voloshin, Bosonic super-WIMPs as keV-scale dark matter, *Phys. Rev. D* **78**, 115012 (2008), arXiv:0807.3279 [hep-ph].
- [106] H. An, M. Pospelov, J. Pradler, and A. Ritz, Direct Detection Constraints on Dark Photon Dark Matter, *Phys. Lett. B* **747**, 331 (2015), arXiv:1412.8378 [hep-ph].
- [107] Y. Hochberg, T. Lin, and K. M. Zurek, Detecting Ultralight Bosonic Dark Matter via Absorption in Superconductors, *Phys. Rev. D* **94**, 015019 (2016), arXiv:1604.06800 [hep-ph].
- [108] Y. Hochberg, T. Lin, and K. M. Zurek, Absorption of light dark matter in semiconductors, *Phys. Rev. D* **95**, 023013 (2017), arXiv:1608.01994 [hep-ph].
- [109] C. Murgui, Y. Wang, and K. M. Zurek, Axion Detection with Optomechanical Cavities, (2022), arXiv:2211.08432 [hep-ph].
- [110] G. Krnjaic and T. Trickle, Absorption of vector dark matter beyond kinetic mixing, *Phys. Rev. D* **108**, 015024 (2023), arXiv:2303.11344 [hep-ph].